Supporting Information

Side-Group Effect of Poly(ε-caprolactone)-Based Polyurethane on Thermal, Surface-Wetting and Mechanical Properties

Zhuoyi He[1], Benshun Huang[1], Kangyu Zhou[2], Jiayi Luo[1], Xi Yang[1], Zhen Wang[1], Limin Ji[1], Yujun Chen[1], Jian Chen[1], Yan Cao[2], Yougen Chen[1*]*

[1] Institute for Advanced Study, Shenzhen University, Nanshan District Shenzhen, Guangdong, 518060, China

[2] Advanced Institute for Soft Matter Science and Technology (AISMST), School of Emergent Soft Matter, South China University of Technology, Guangzhou, 510640, China

CORRESPONDING AUTHOR FOOTNOTE

Tel & Fax: +86-75526943283.

E-mail: crystinacao@scut.edu.cn (Y. Cao); chenyg@szu.edu.cn (Y.-G. Chen)

Experimental Section

Scheme S1. Synthesis of 2-(bromomethyl)-2-methylpropane-1,3-diol

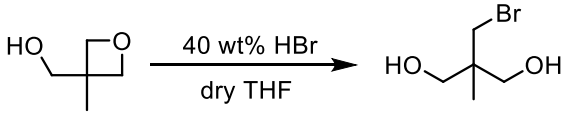

(3-methyloxetan-3-yl)methanol 2-(bromomethyl)-2-methylpropane-1,3-diol

Synthesis of 2-(bromomethyl)-2-methylpropane-1,3-diol. In a 1000 mL three-necked flask, (3-methyloxetan-3-yl)methanol (25.03 g, 0.2451 mol) and dry THF (200 mL) were sequentially added. Under ice bath conditions, 100 mL of 40 wt% hydrobromic acid was slowly dropped and reacted at room temperature for 6 hours. After the reaction was complete, saturated sodium bicarbonate solution was added to adjust the pH to neutral. The mixed solution was then poured into a separatory funnel and extracted with 3 × 300 mL of ethyl acetate. The mixture was dried over anhydrous sodium sulfate, and the ethyl acetate was removed under reduced pressure. It was then recrystallized in *n*-hexane/ether to obtain white crystals of 2-(bromomethyl) -2-methylpropane-1,3-diol (29.87 g, yield 74%). ^{1}H NMR (400 MHz, $CDCl_3$, δ) 3.67 (s, -C(C*H*$_2$OH)$_2$, 4H), 3.55 (s, -C*H*$_2$Br, 2H), 0.93 (s, -C*H*$_3$, 3H). ^{13}C NMR (60 MHz, $CDCl_3$, δ) 68.3 (-C(*C*H$_2$OH)$_2$, 2C), 40.7 (-*C*(CH$_2$OH)$_2$, 1C), 39.3 (-*C*H$_2$Br, 1C), 18.5 (-*C*H$_3$, 1C). ESI-MS $[M + H]^+$ calculated: 183.00, found: 183.00.

Scheme S2. Synthesis of 2-(azidomethyl)-2-methylpropane-1,3-diol (**1**)

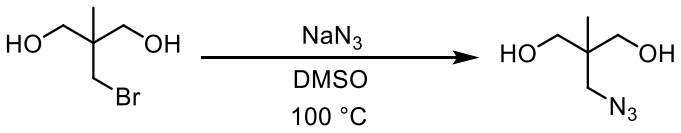

2-(bromomethyl)-2-methylpropane-1,3-diol 2-(azidomethyl)-2-methylpropane-1,3-diol

Synthesis of 2-(azidomethyl)-2-methylpropane-1,3-diol. In a 100 mL three-necked flask, 2-(bromomethyl)-2-methylpropane-1,3-diol (6.36 g, 34.75 mmol), NaN_3 (4.5 g, 69.2 mmol), and DMSO (45 mL) were added. The reaction mixture was heated to 100 ℃ and kept for 12 hours. Most of DMSO was removed by rotary evaporation. 50 mL of saturated sodium chloride solution was added into the residue was and extracted with 3 × 100 mL of ether. The organic phase was dried with anhydrous sodium sulfate and the salt was filtered. The solvent was removed and fresh ether was

added for recrystallization to afford white crystalline **1** (3.5 g, 24.1 mmol) with a yield of 70%. ^{1}H NMR (400 MHz, $CDCl_3$, δ) 3.59 (s, -C(C*H*$_2$OH)$_2$, 4H), 3.44 (s, -C*H*$_2$N$_3$, 2H), 0.86 (s, -C*H*$_3$, 3H). ^{13}C NMR (60 MHz, $CDCl_3$, δ) 67.9 (-C(*C*H$_2$OH)$_2$, 2C), 55.6 (-*C*H$_2$N$_3$, 1C), 41.0 (-*C*(CH$_2$OH)$_2$, 1C), 17.6 (-*C*H$_3$, 1C). ESI-MS $[M + H]^+$ calculated: 146.09, found: 146.09.

Scheme S3. Synthesis of 2,5,8,11-tetraoxatetradec-13-yne

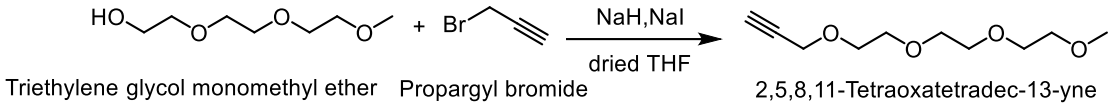

Triethylene glycol monomethyl ether Propargyl bromide 2,5,8,11-Tetraoxatetradec-13-yne

Synthesis of 2,5,8,11-tetraoxatetradec-13-yne. Triethylene glycol monomethyl ether (TGME, 4.77 mL, 30.5 mmol) and anhydrous THF (100 mL) were added into a 500 mL three necked flask, and the mixture was stirred under argon for 10 min. NaH (2.7 g, 60 mmol) and NaI (225 mg, 1.5 mmol) were then added and the mixture was stirred for several minutes. Afterwards, propargyl bromide (5 mL, 45.5 mmol) was added by syringe and the reaction mixture was further stirred at room temperature for 16 hours. The reaction mixture was poured into a separatory funnel, extracted with saturated NaCl twice, ethyl acetate twice, and distilled water once, dried over anhydrous Na_2SO_4. Ethyl acetate was removed under reduced pressure, and the residue was passed through a short silica column with dichloromethane to afford the final product as an orange red liquid (Yield: 95%). ^{1}H NMR (400 MHz, $CDCl_3$, δ) 4.17 (-C*H*$_2$C≡CH, 2H), 3.70-3.50 (-OC*H*$_2$C*H*$_2$O-, 12H), 3.34 (-OC*H*$_3$, 3H), 2.40 (-C≡C*H*, 1H).^{13}C NMR (400 MHz, $CDCl_3$, δ) 79.7 (-CH$_2$*C*≡CH, 1C), 74.5 (-CH$_2$C≡*C*H, 1C), 72.0 (-*C*H$_2$OCH$_3$, 1C), 70.3-70.8 (-O*C*H$_2$*C*H$_2$O*C*H$_2$CH$_2$OCH$_3$, 3C), 69.2 (-O*C*H$_2$*C*H$_2$OCH$_2$C≡CH, 2C), 59.1 (-*C*H$_2$C≡CH, 1C), 58.4 (-*C*H$_3$, 1C). ESI-MS $[M + H]^+$ calculated: 203.13, found: 203.13.

Scheme S4. Synthesis of 3,6,9,12-Tetraoxapentadec-14-yne

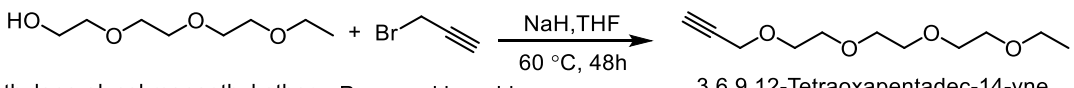

Triethylene glycol monoethyl ether Propargyl bromide 3,6,9,12-Tetraoxapentadec-14-yne

Synthesis of 3,6,9,12-Tetraoxapentadec-14-yne. Triethylene glycol monoethyl ether (4.12 g, 23.12 mmol) and anhydrous THF (100 mL) were added into a 500 mL three

necked flask, and the whole mixture was stirred under argon for 10 min. NaH (2.7 g, 60 mmol) and NaI (225 mg, 1.5 mmol) were then added and the mixture was stirred for a few minutes. Afterwards, propargyl bromide (5 mL, 45.5 mmol) was added by syringe and the reaction mixture was further stirred at room temperature for 16 hours. The reaction mixture was poured into a separatory funnel, extracted with saturated NaCl twice, ethyl acetate twice, and distilled water once, dried over anhydrous Na_2SO_4. Ethyl acetate was removed under reduced pressure, and the residue was passed through a short silica column with EtOAc/CH_2Cl_2 = 1:1 (v/v) to afford the final product as a slightly orange liquid (Yield: 66 %). ^{1}H NMR (400 MHz, $CDCl_3$, δ) 4.10 (-C*H*$_2$C≡CH, 2H), 3.70-3.50 (-OC*H*$_2$C*H*$_2$O-, 12H), 3.34 (-OC*H*$_2$CH$_3$, 2H), 2.41 (-C≡C*H*, 1H), 1.20 (-C*H*$_3$, 3H). ^{13}C NMR (400 MHz, $CDCl_3$, δ) 79.7 (-CH$_2$*C*≡CH, 1C), 74.5 (-CH$_2$C≡*C*H, 1C), 69.8-70.8 (-OCH$_2$*C*H$_2$O*C*H$_2$*C*H$_2$O*C*H$_2$*C*H$_2$OCH$_3$, 5C), 69.1 (-CH$_2$*C*H$_2$OCH$_3$, 1C), 66.7 (-*C*H$_2$CH$_3$, 1C), 58.5 (-*C*H$_2$-C≡CH, 1C), 15.2 (-CH$_2$*C*H$_3$, 1C). ESI-MS $[M + H]^+$ calculated: 217.14, found: 217.14.

Scheme S5. Synthesis of 4-(4-ethynylphenyl)pyridine.

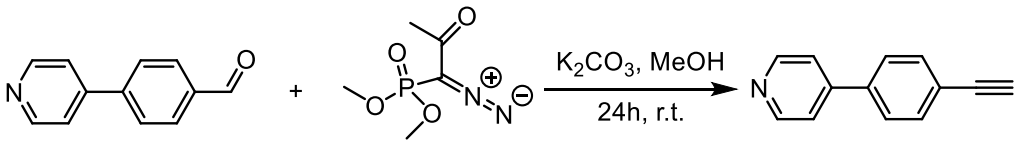

4-(4-Pyridinyl)benzaldehyde Bestmann-Ohira reagent 4-(4-ethynylphenyl)pyridine

Synthesis of 4-(4-ethynylphenyl)pyridine. In a 100 mL three necked flask, 4-(4-pyridinyl)benzaldehyde (1.70 g, 9.28 mmol) was dissolved in anhydrous methanol (15 mL) under Argon and diluted with ethyl acetate (30 mL). The mixture was stirred for 10 min. Afterwards, K_2CO_3 (3.4 g, 24.6 mmol) and Bestmann-Ohira agent (3.4 g, 17.7 mmol) were added and the reaction mixture was further stirred for 24 hours. The solvent was removed and the residue was dissolved in CH_2Cl_2. The solution was washed with saturated ammonium chloride thrice and the organic layer was dried with anhydrous Na_2SO_4. CH_2Cl_2 was removed by evaporation and the residue was passed through a silica chromatography (EtOAc/hexane = 1:2, v/v) to afford 4-(4-ethynylphenyl)pyridine as white solid (Yield: 60.2%). ^{1}H NMR (400 MHz, $CDCl_3$, δ) 8.67 (pyridyl H, 2H), 7.60 (phenyl, 4H), 7.49 (pyridyl H, 2H), 3.18 (-C≡C*H*, 1H). ^{13}C NMR (400 MHz, $CDCl_3$, δ) 150.35 (pyridyl C, 2C), 147.42

(pyridyl C, 1C), 138.39 (phenyl C, 1C), 132.80 (phenyl C, 2C), 126.96 (phenyl C, 2C), 122.94 (phenyl C, 1C), 121.53 (pyridyl C, 2C), 82.97 (-*C*≡CH, 1C), 78.71 (-C≡*C*H, 1C). ESI-MS $[M + H]^+$ calculated: 180.08, found: 180.17.

Tables and Figures

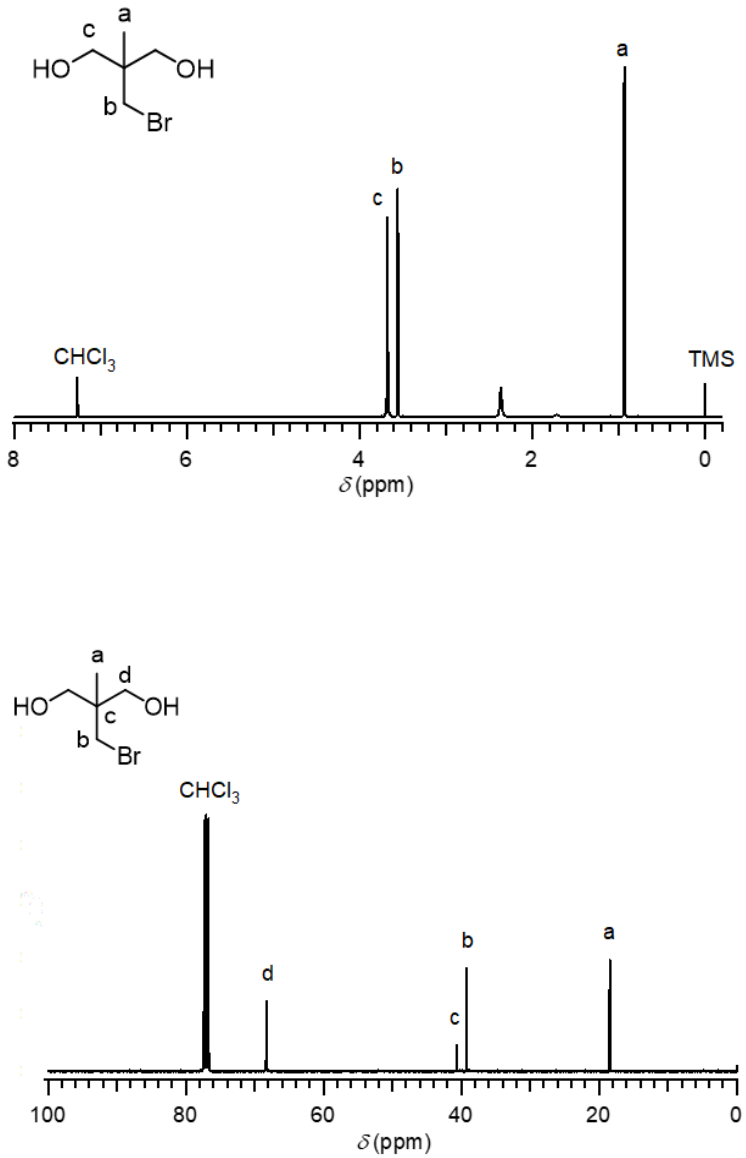

Figure S1. ^{1}H and ^{13}C NMR spectra of 2-(bromomethyl)-2-methylpropane-1,3-diol in $CDCl_3$.

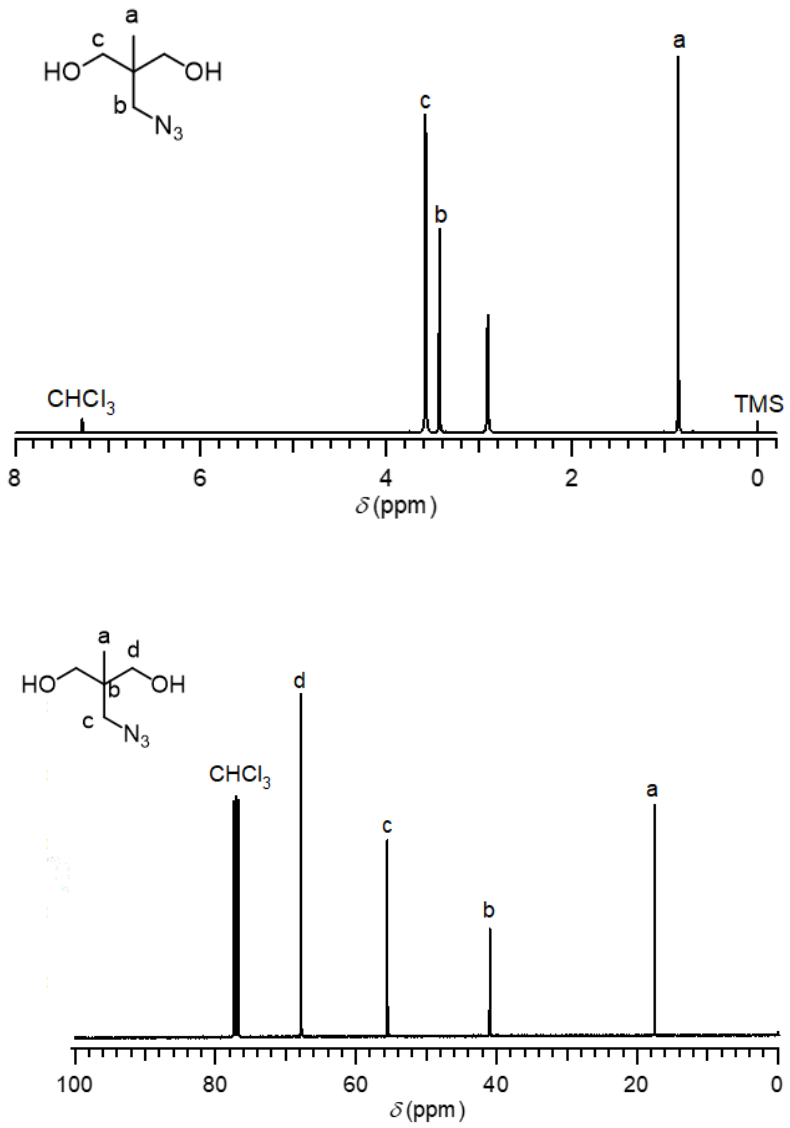

Figure S2. ^{1}H and ^{13}C NMR spectra of 2-(azidomethyl)-2-methylpropane-1,3-diol in $CDCl_3$.

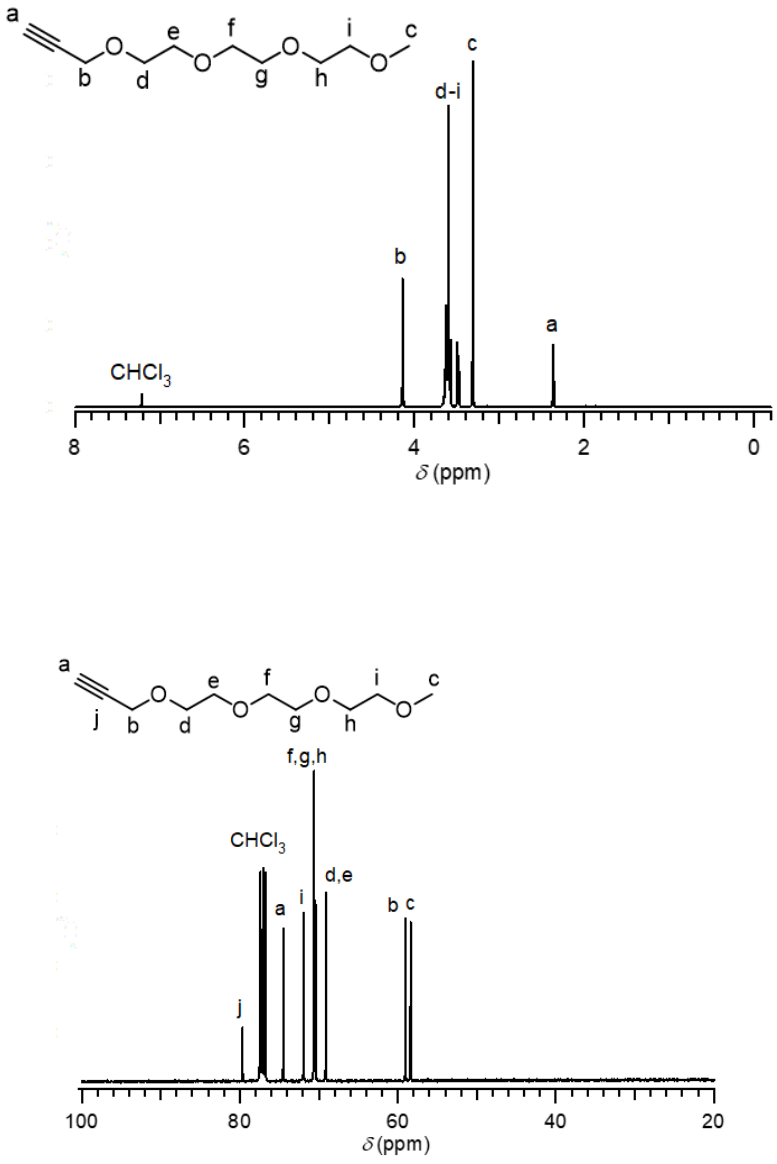

Figure S3. ^{1}H and ^{13}C NMR spectrum of 2,5,8,11-tetraoxatetradec-13-yne in $CDCl_3$.

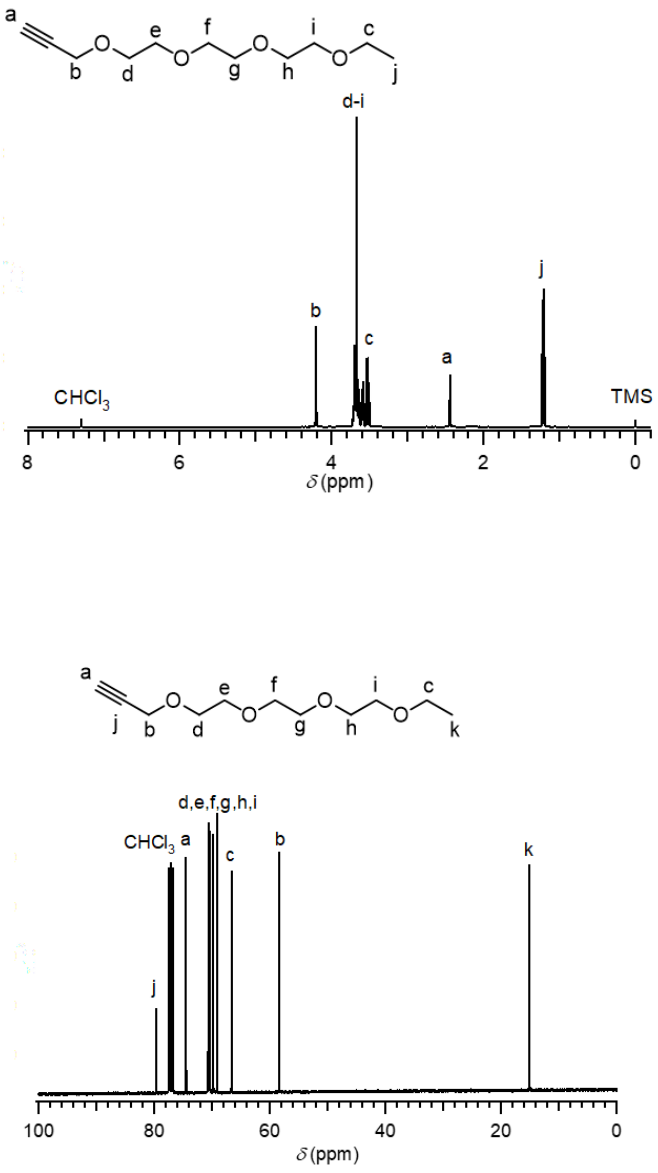

Figure S4. ^{1}H and ^{13}C NMR spectrum of 3,6,9,12-tetraoxapentadec-14-yne in $CDCl_3$.

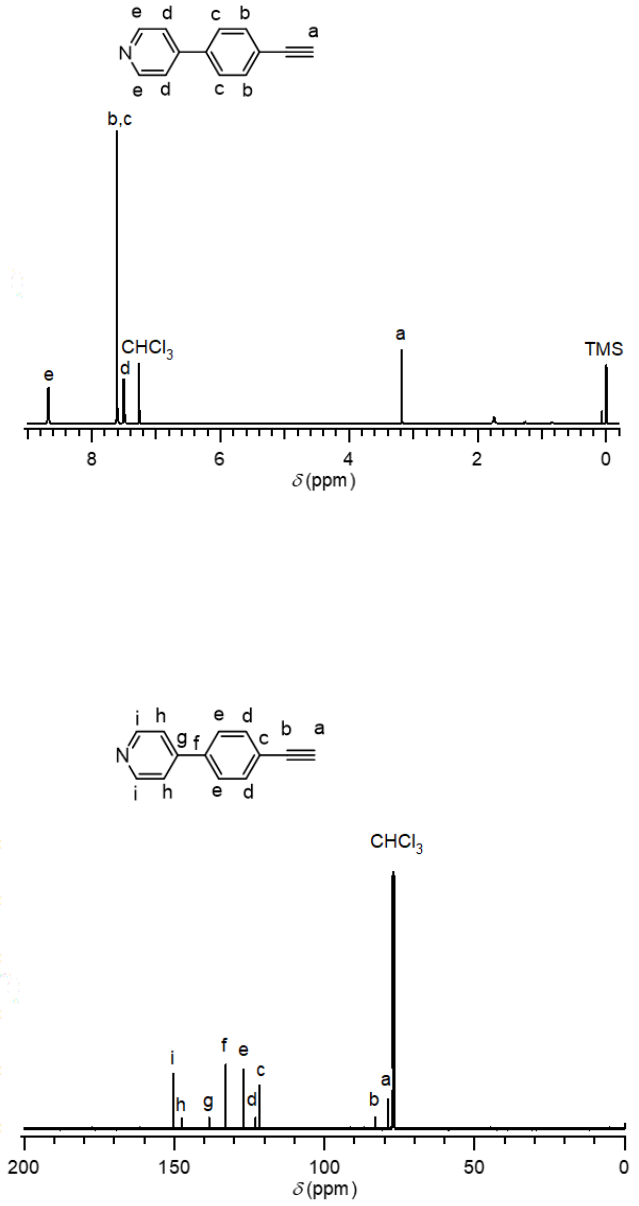

Figure S5. ^{1}H and ^{13}C NMR spectra of 4-(4-ethynylphenyl) pyridine in $CDCl_3$.

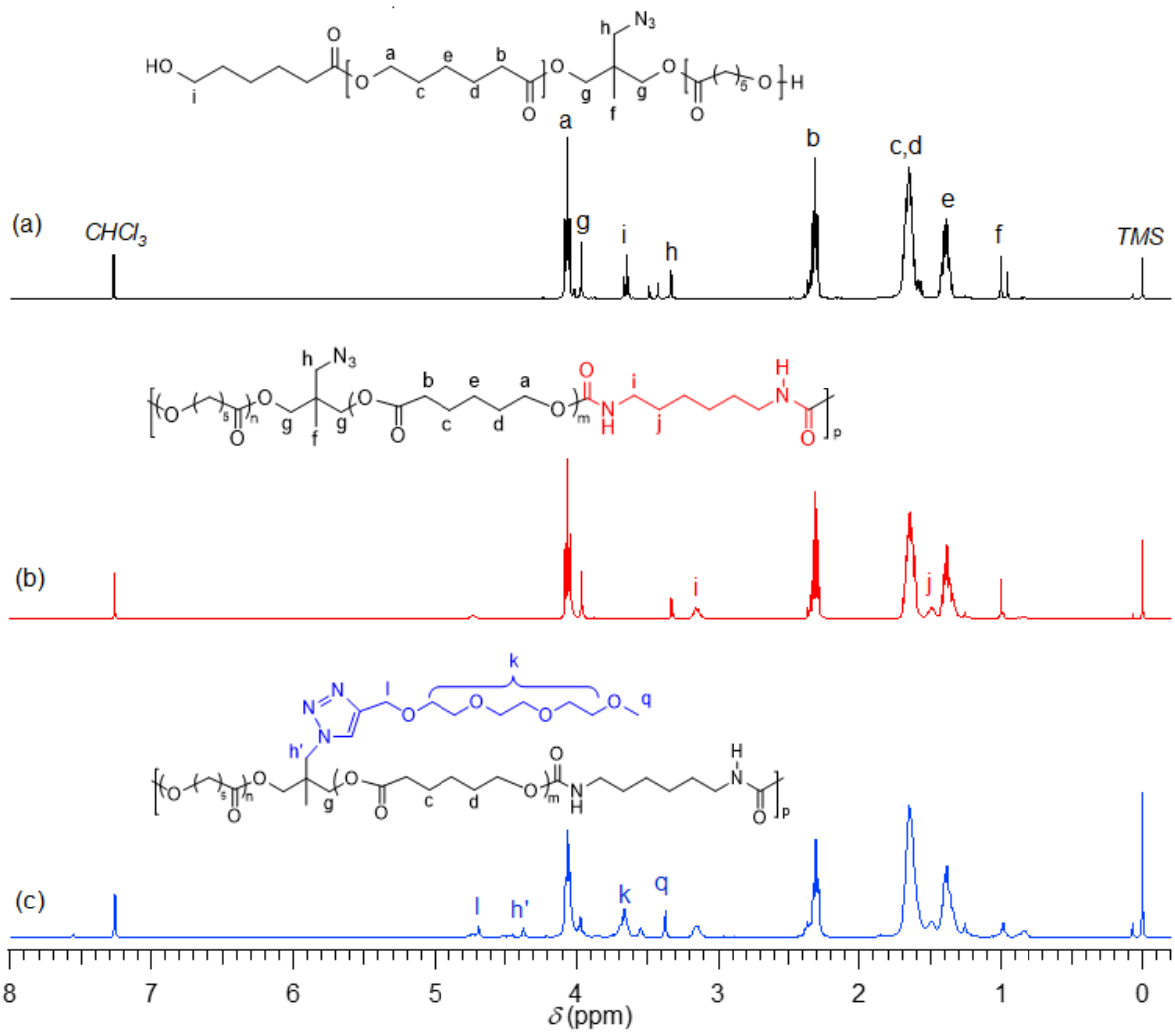

Figure S6. ^{1}H NMR spectra of PCL_{10}-N_3 (a), PU_{10}-N_3 (b) and PU_{10}-1 (c) determined in $CDCl_3$ at r.t.

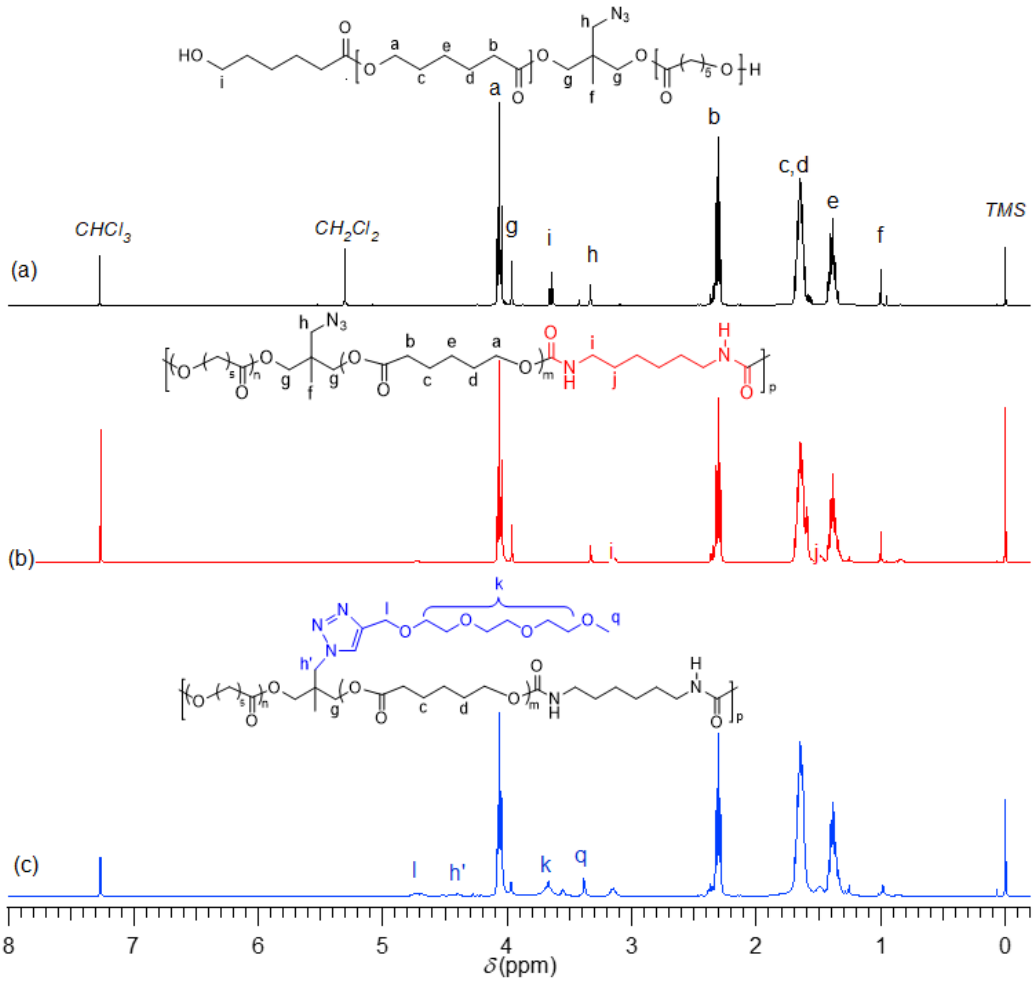

Figure S7. ^{1}H NMR spectra of PCL_{20}-N_3 (a), PU_{20}-N_3 (b) and PU_{20}-1 (c) determined in $CDCl_3$ at r.t.

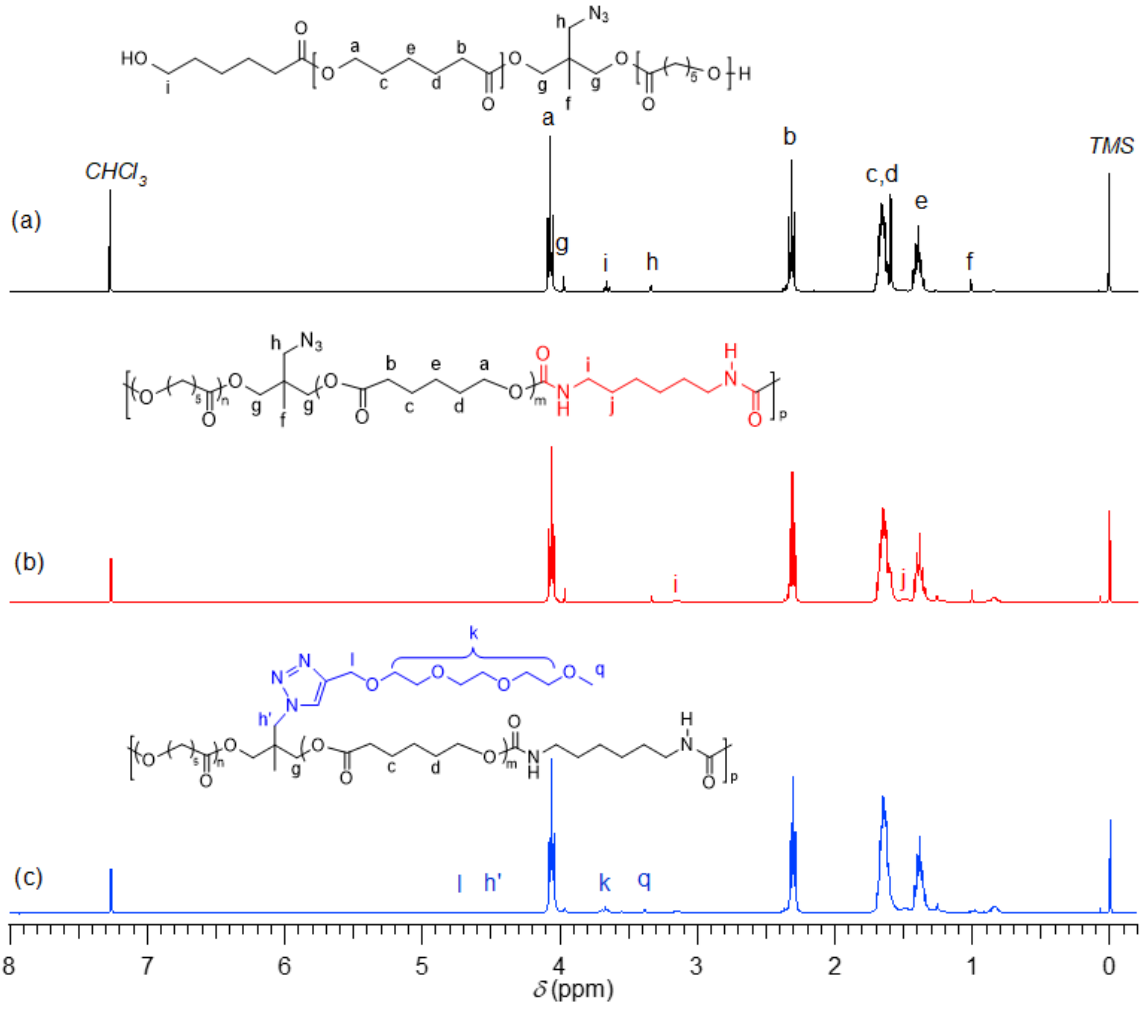

Figure S8. ^{1}H NMR spectra of PCL_{40}-N_3 (a), PU_{40}-N_3 (b) and PU_{40}-1 (c) determined in $CDCl_3$ at r.t.

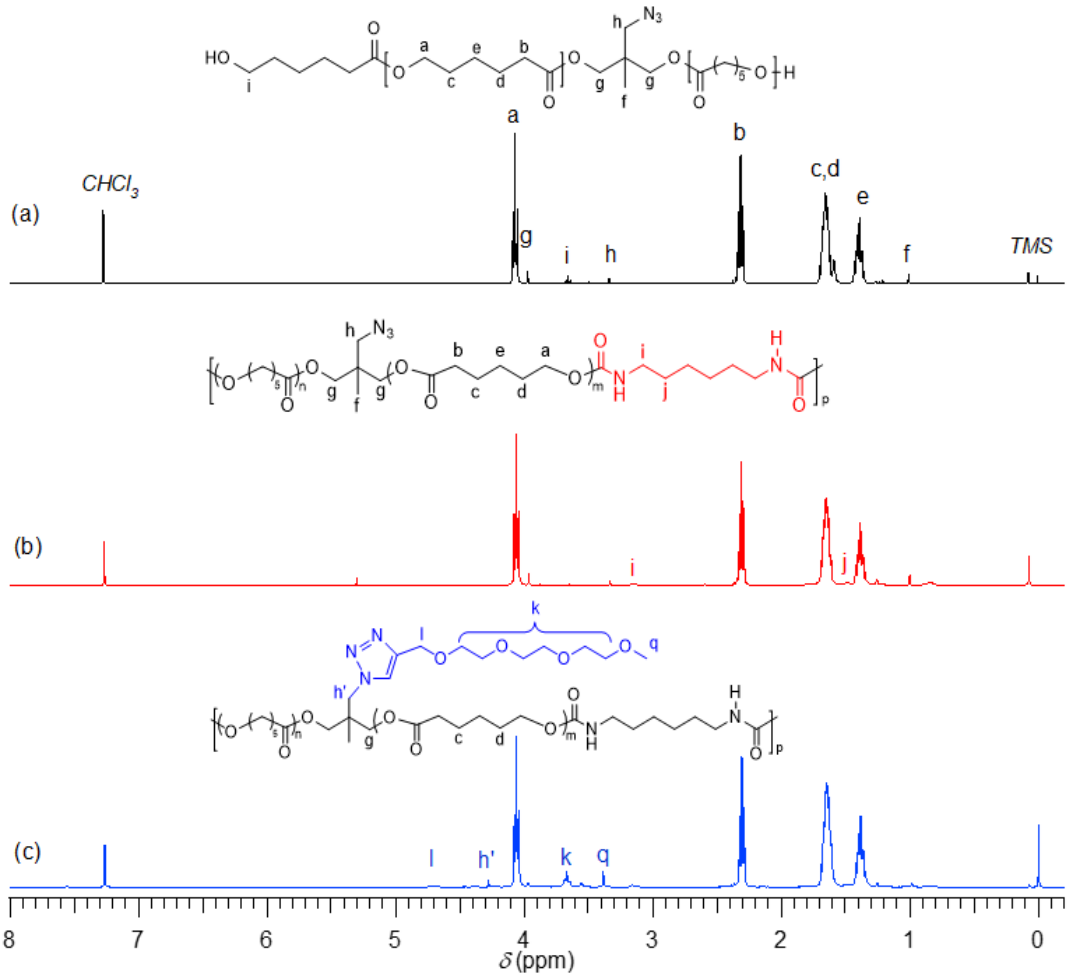

Figure S9. ^{1}H NMR spectra of PCL_{50}-N_3 (a), PU_{50}-N_3 (b) and PU_{50}-1 (c) determined in $CDCl_3$ at r.t.

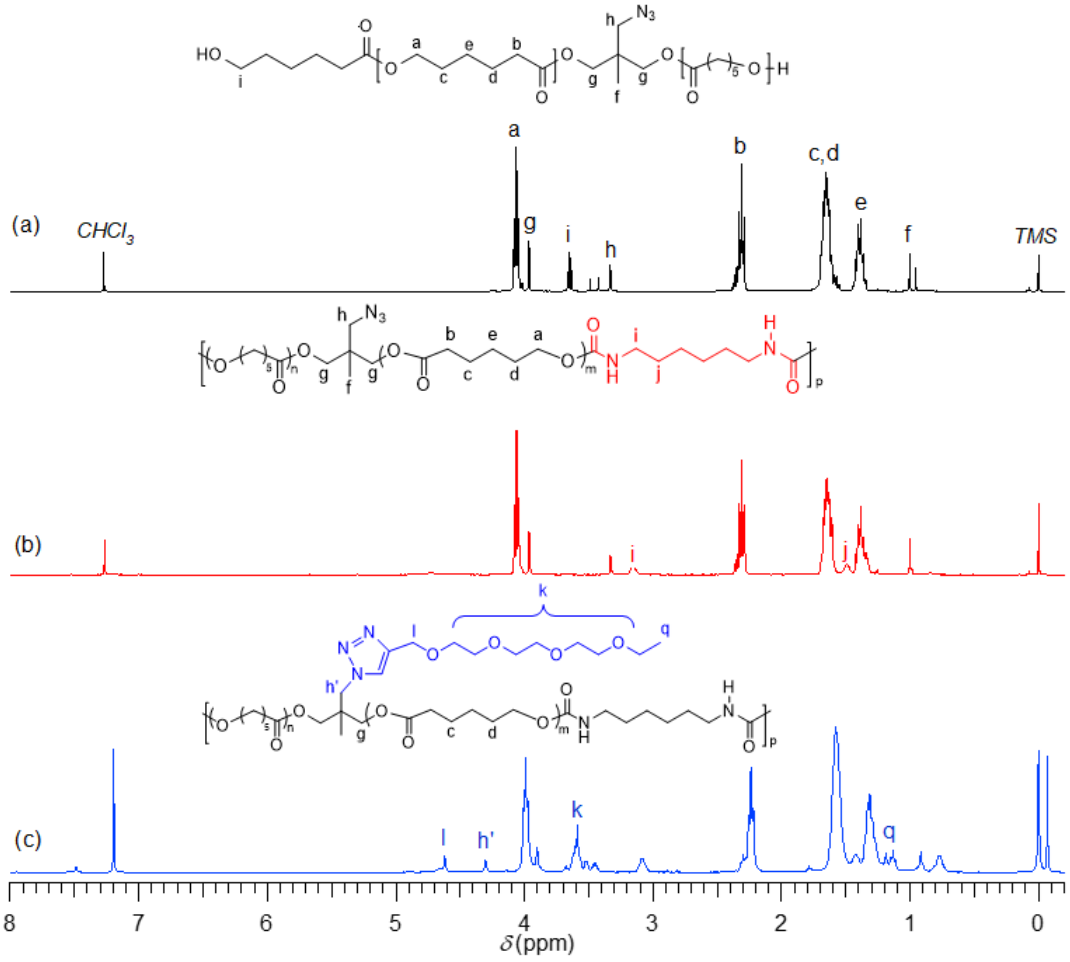

Figure S10. ^{1}H NMR spectra of PCL_{10}-N_3 (a), PU_{10}-N_3 (b) and PU_{10}-2 (c) determined in $CDCl_3$ at r.t.

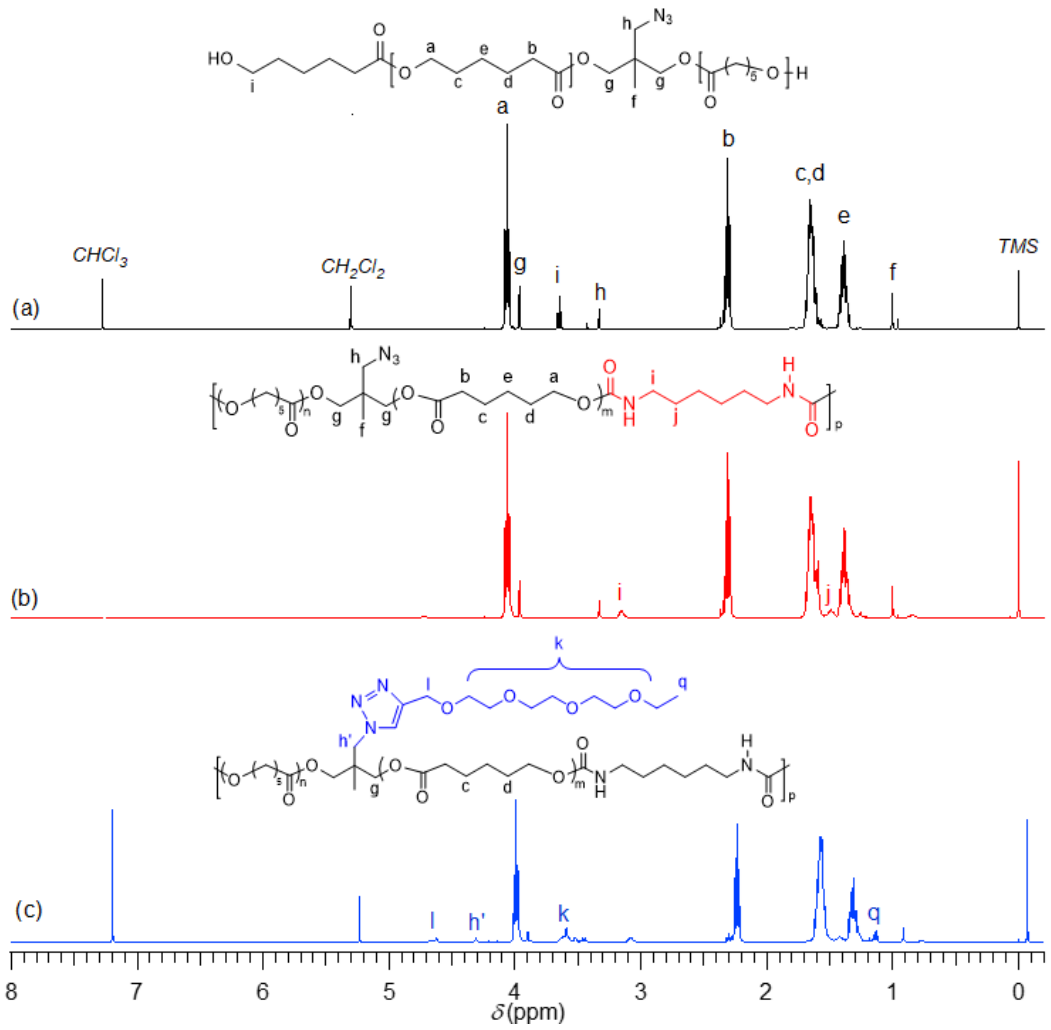

Figure S11. ^{1}H NMR spectra of PCL_{20}-N_3 (a), PU_{20}-N_3 (b) and PU_{20}-2 (c) determined in $CDCl_3$ at r.t.

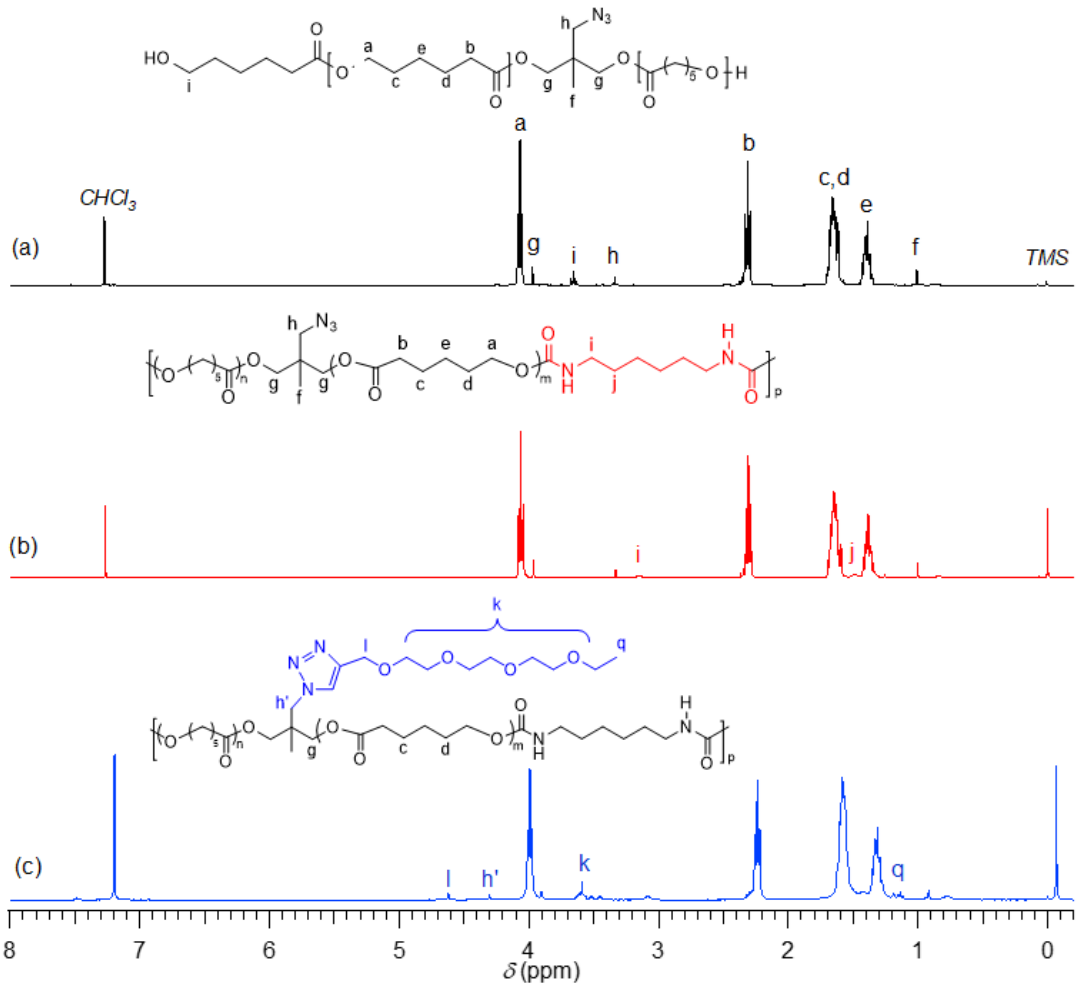

Figure S12. ^{1}H NMR spectra of PCL_{30}-N_3 (a), PU_{30}-N_3 (b) and PU_{30}-2 (c) determined in $CDCl_3$ at r.t.

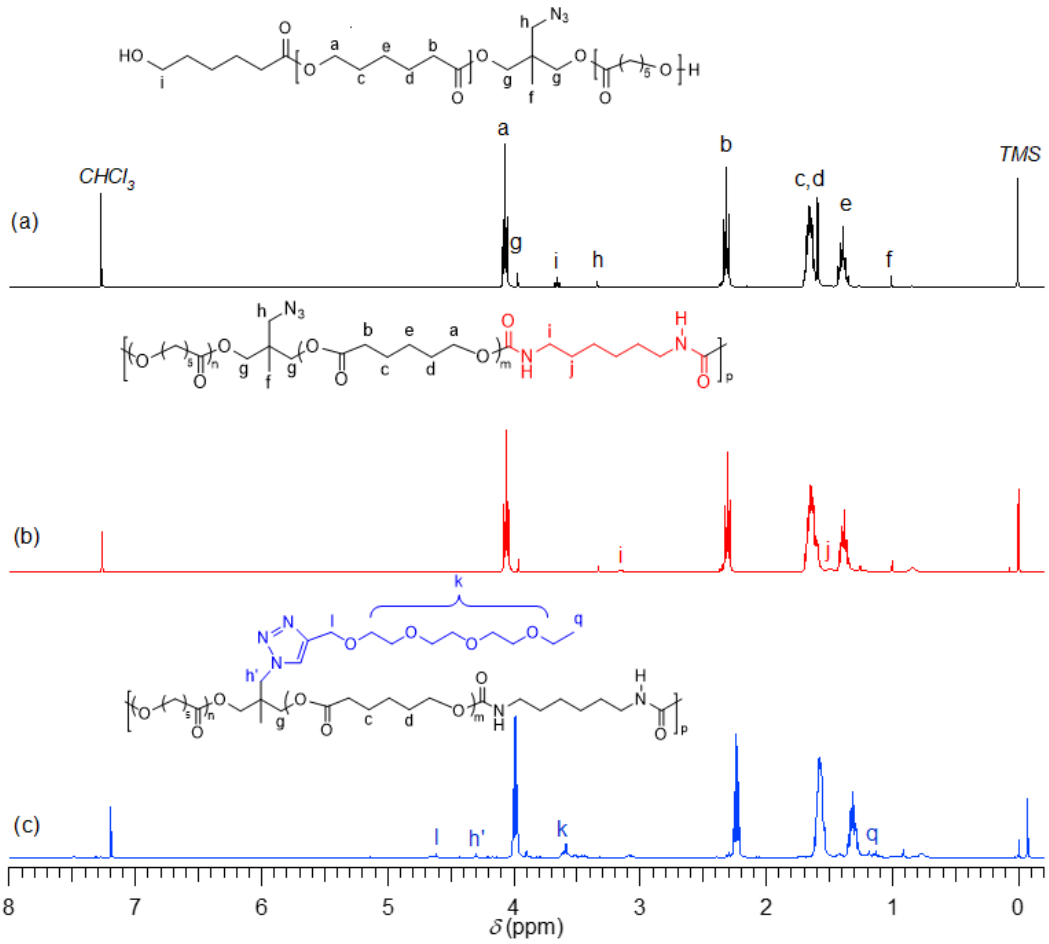

Figure S13. ^{1}H NMR spectra of PCL_{40}-N_3 (a), PU_{40}-N_3 (b) and PU_{40}-2 (c) determined in $CDCl_3$ at r.t.

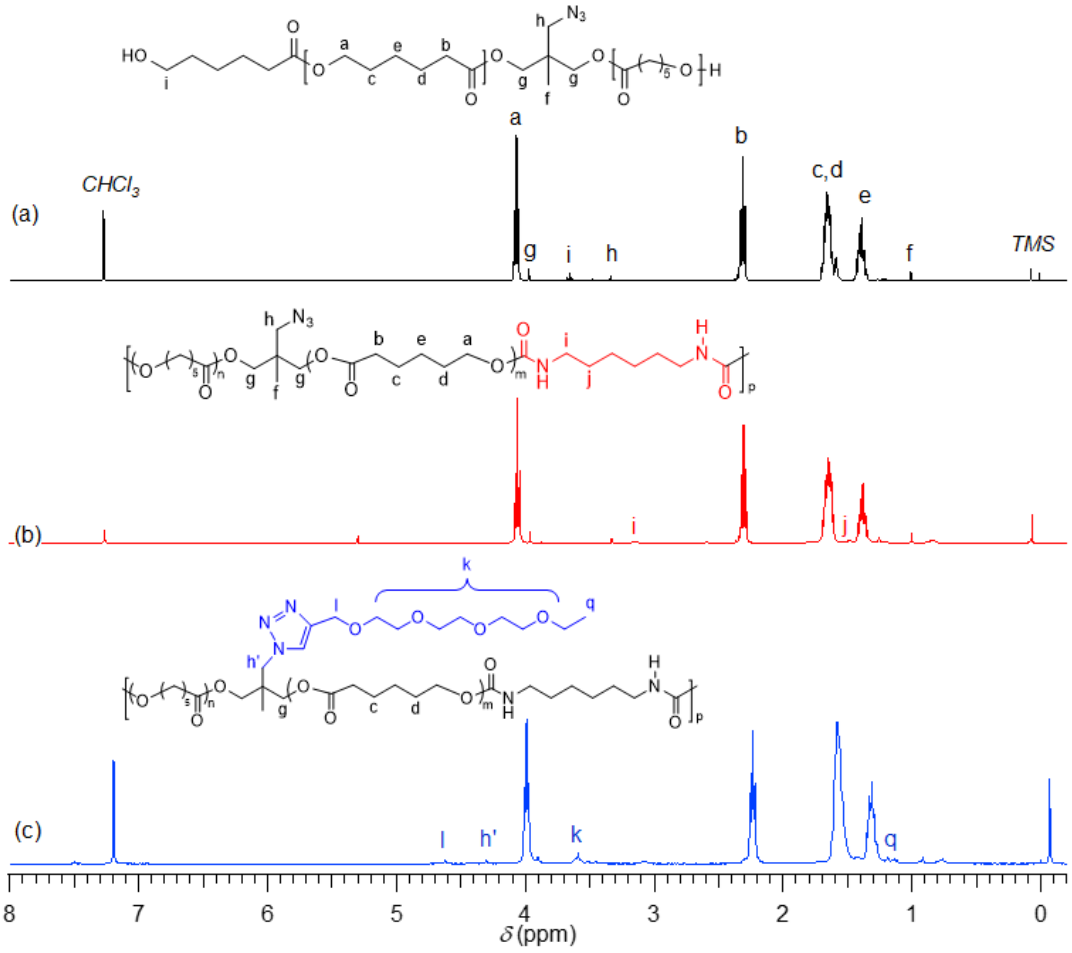

Figure S14. ^{1}H NMR spectra of PCL_{50}-N_3 (a), PU_{50}-N_3 (b) and PU_{50}-2 (c) determined in $CDCl_3$ at r.t.

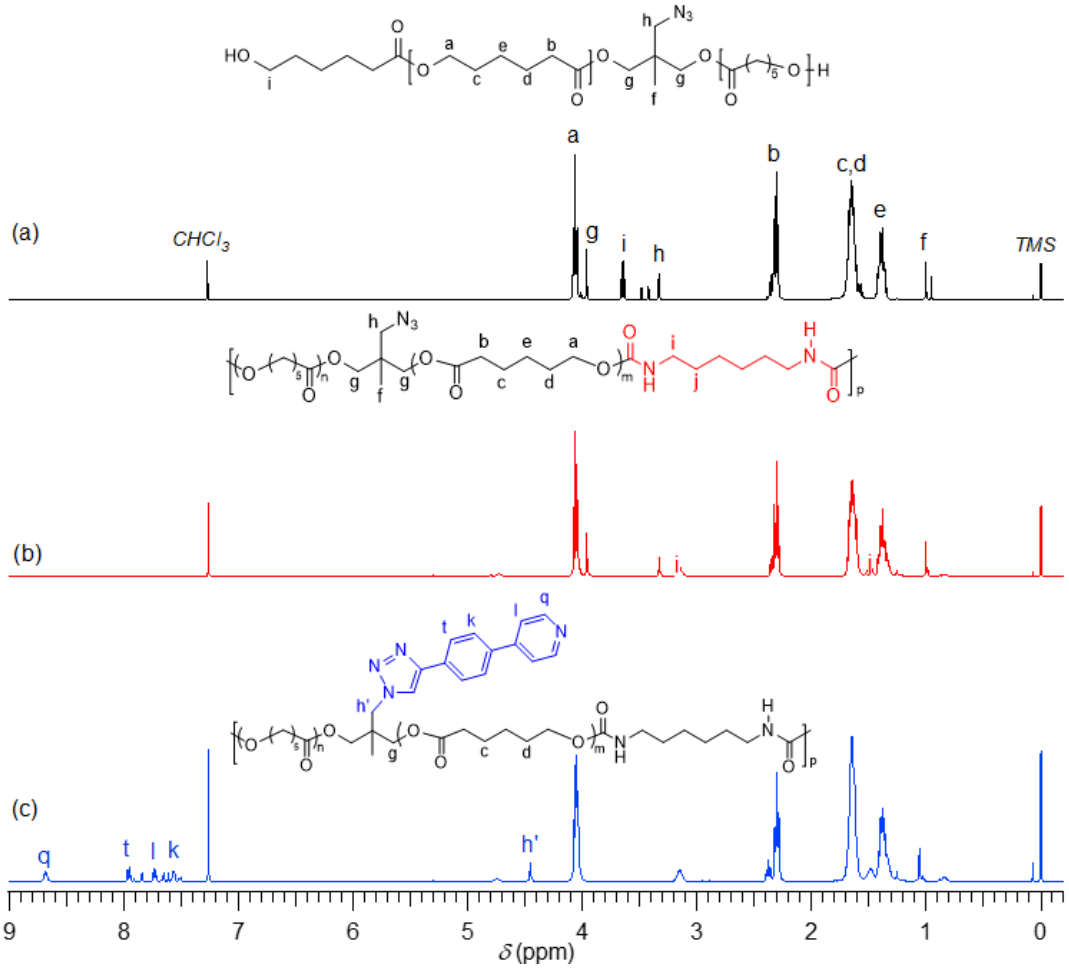

Figure S15. ^{1}H NMR spectra of PCL_{10}-N_3 (a), PU_{10}-N_3 (b) and PU_{10}-3 (c) determined in $CDCl_3$ at r.t.

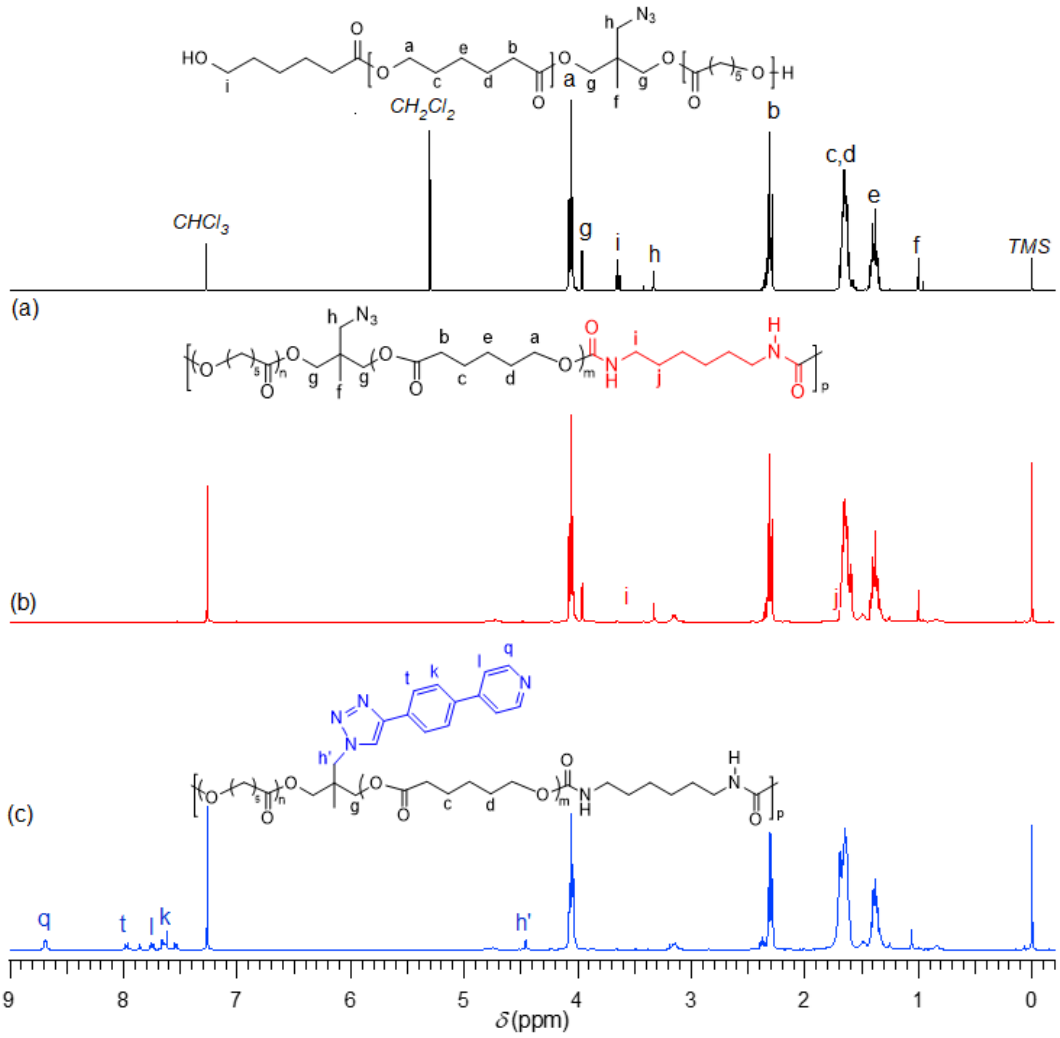

Figure S16. ^{1}H NMR spectra of PCL_{20}-N_3 (a), PU_{20}-N_3 (b) and PU_{20}-3 (c) determined in $CDCl_3$ at r.t.

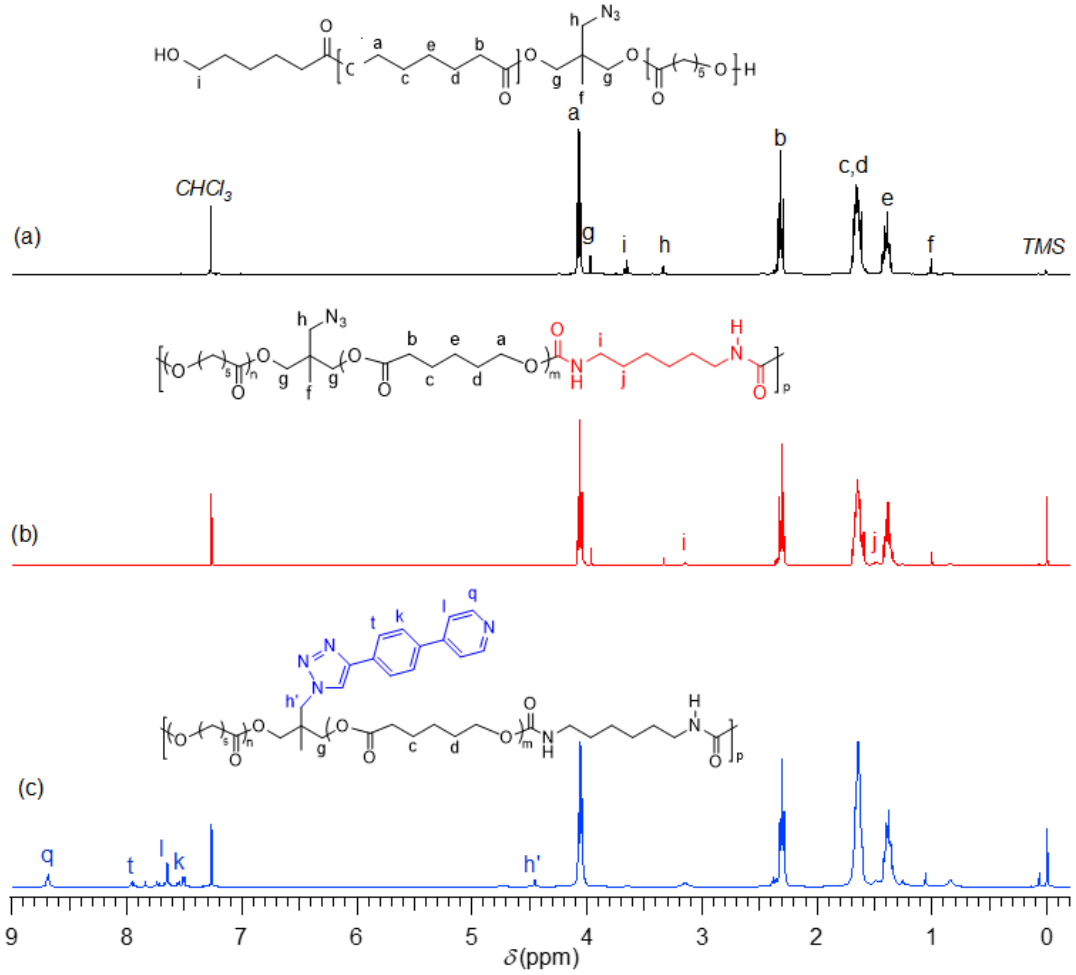

Figure S17. ^{1}H NMR spectra of PCL_{30}-N_3 (a), PU_{30}-N_3 (b) and PU_{30}-3 (c) determined in $CDCl_3$ at r.t.

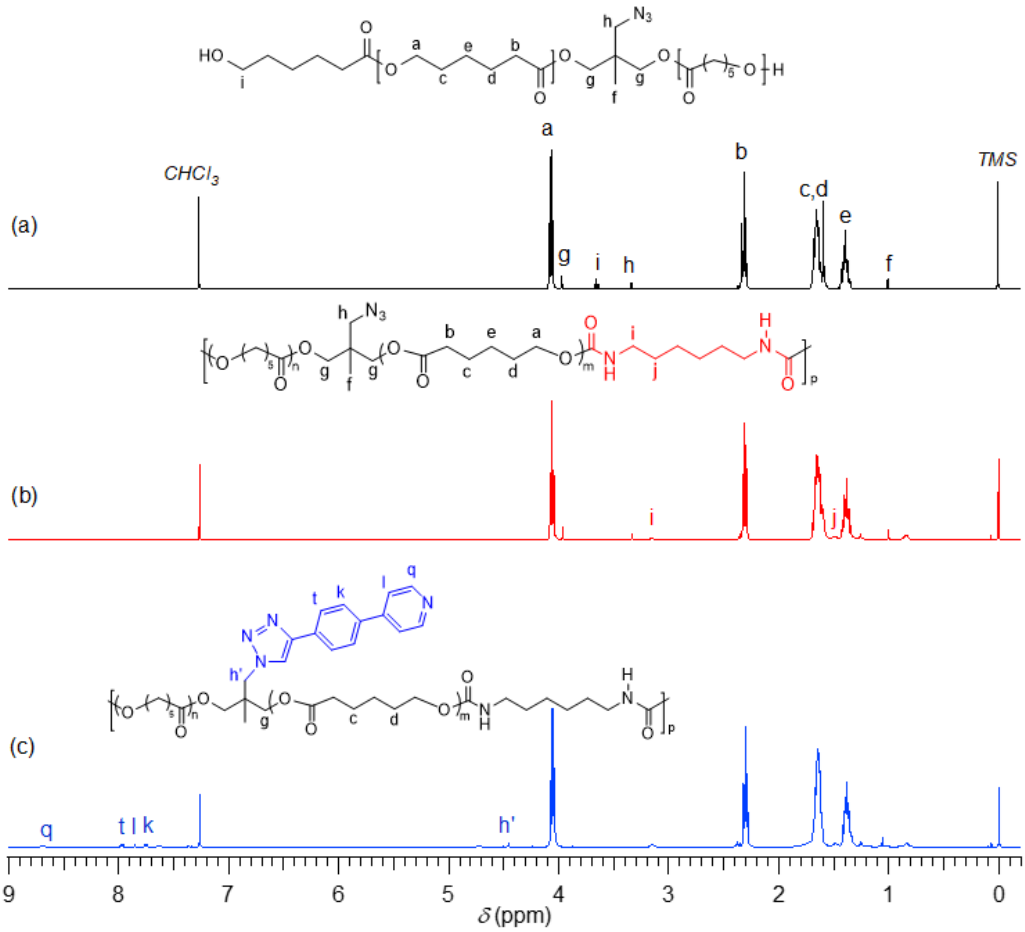

Figure S18. ^{1}H NMR spectra of PCL_{40}-N_3 (a), PU_{40}-N_3 (b) and PU_{40}-3 (c) determined in $CDCl_3$ at r.t.

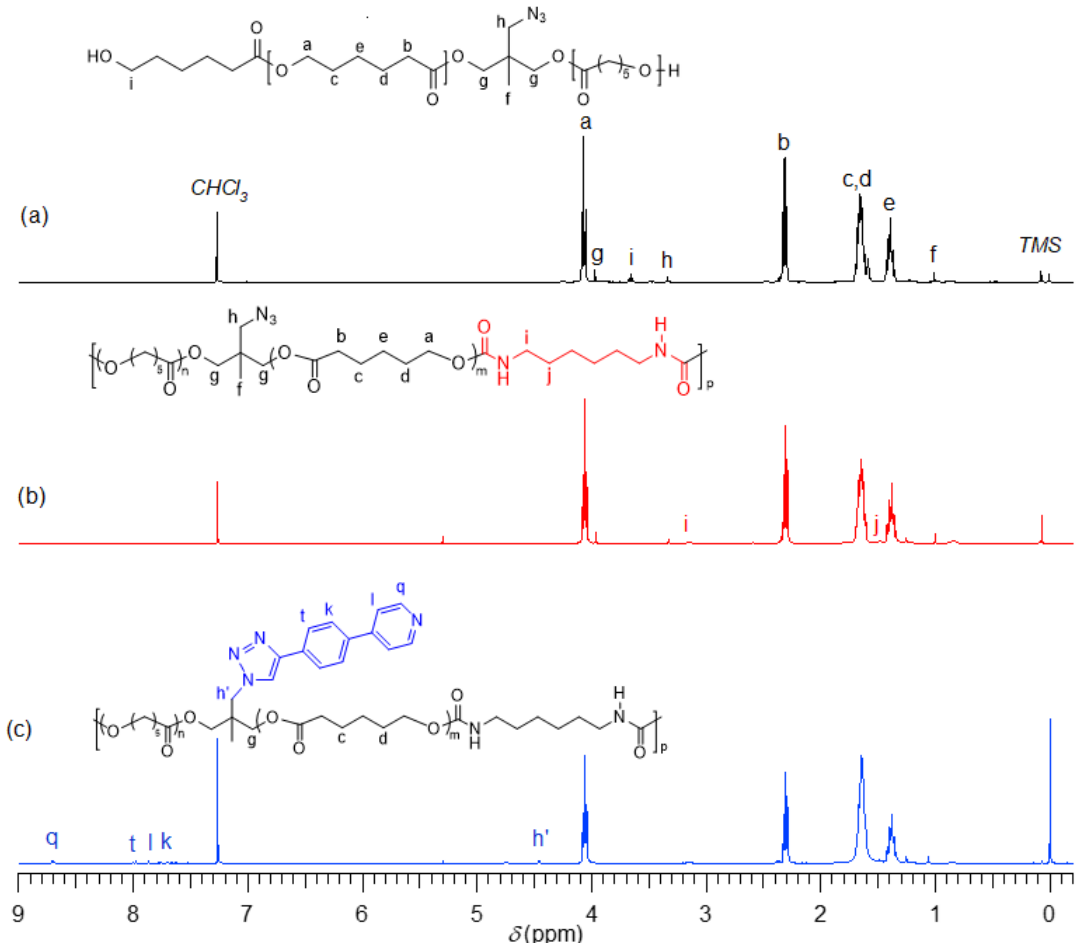

Figure S19. ^{1}H NMR spectra of PCL_{50}-N_3 (a), PU_{50}-N_3 (b) and PU_{50}-3 (c) determined in $CDCl_3$ at r.t.

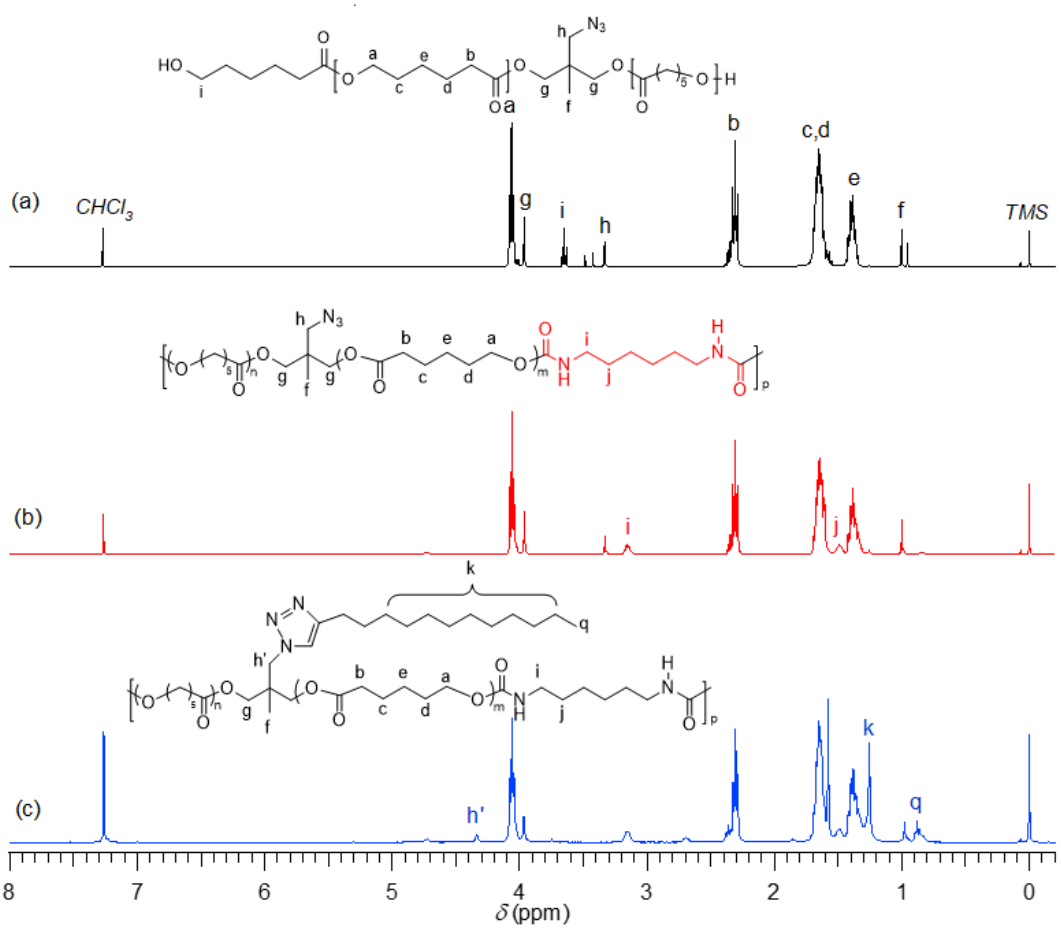

Figure S20. ^{1}H NMR spectra of PCL_{10}-N_3 (a), PU_{10}-N_3 (b) and PU_{10}-4 (c) determined in $CDCl_3$ at r.t.

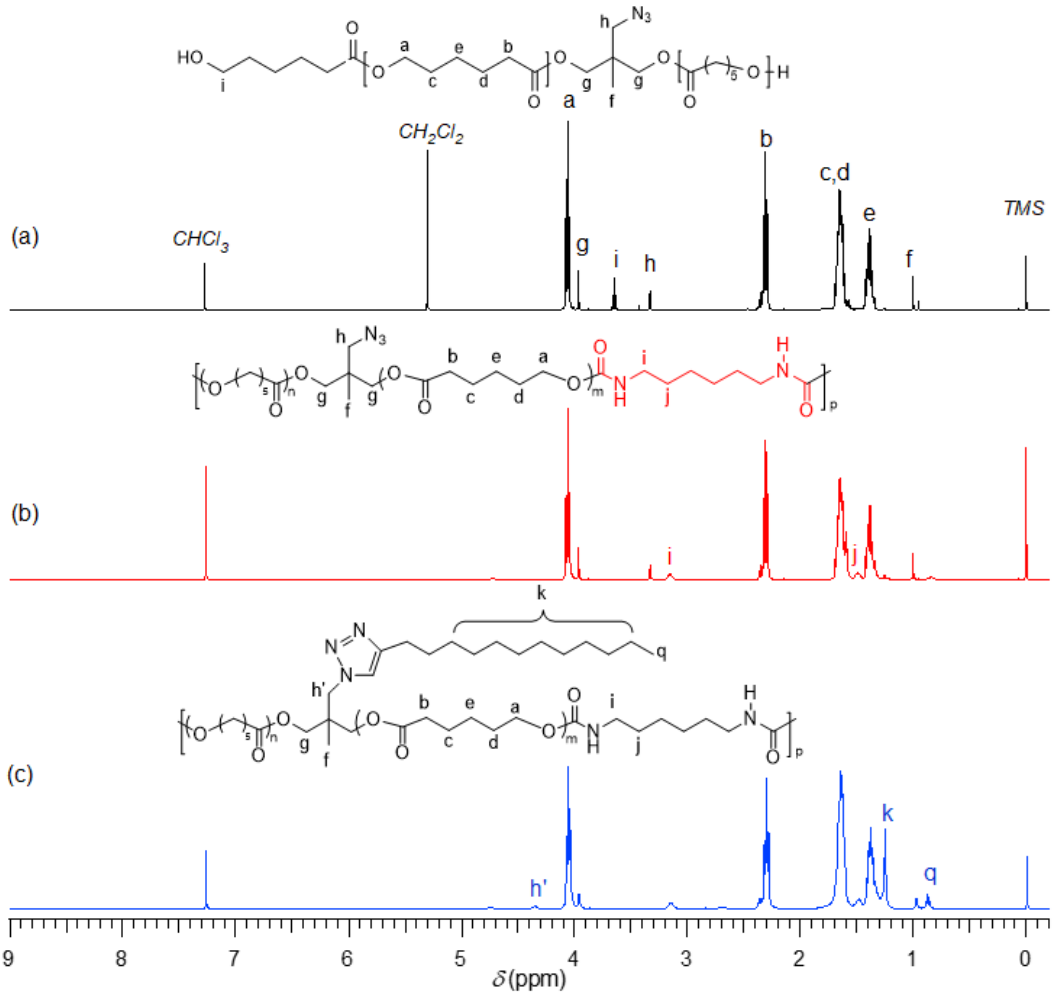

Figure S21. ^{1}H NMR spectra of PCL_{20}-N_3 (a), PU_{20}-N_3 (b) and PU_{20}-4 (c) determined in $CDCl_3$ at r.t.

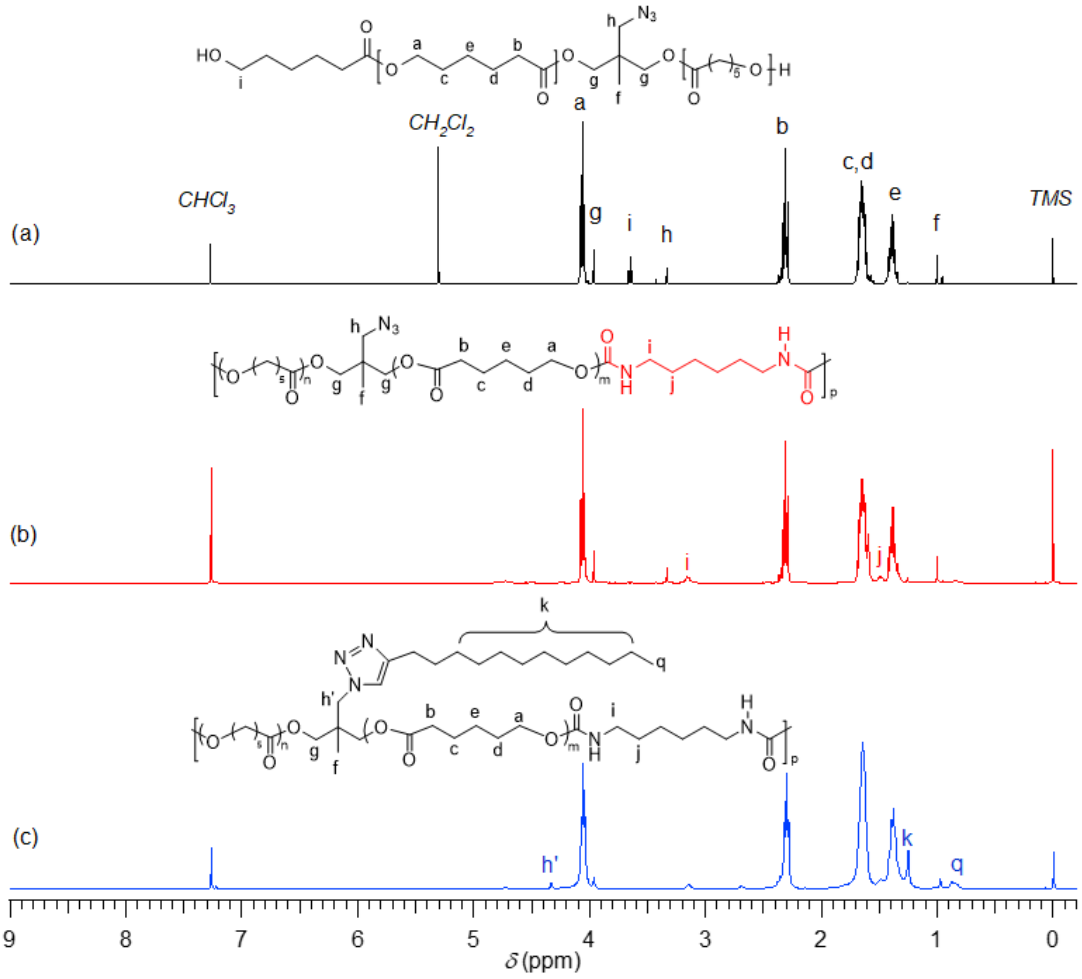

Figure S22. ^{1}H NMR spectra of PCL_{30}-N_3 (a), PU_{30}-N_3 (b) and PU_{30}-4 (c) determined in $CDCl_3$ at r.t.

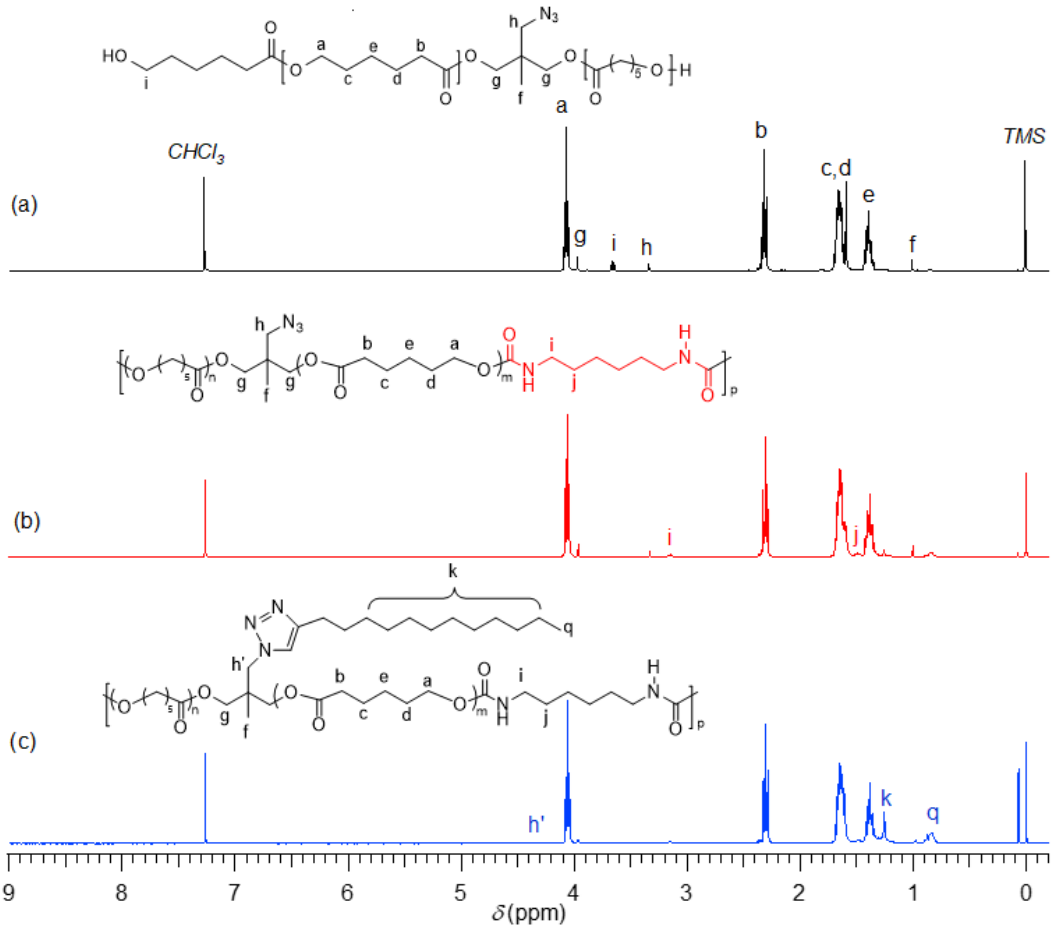

Figure S23. ^{1}H NMR spectra of PCL_{40}-N_3 (a), PU_{40}-N_3 (b) and PU_{40}-4 (c) determined in $CDCl_3$ at r.t.

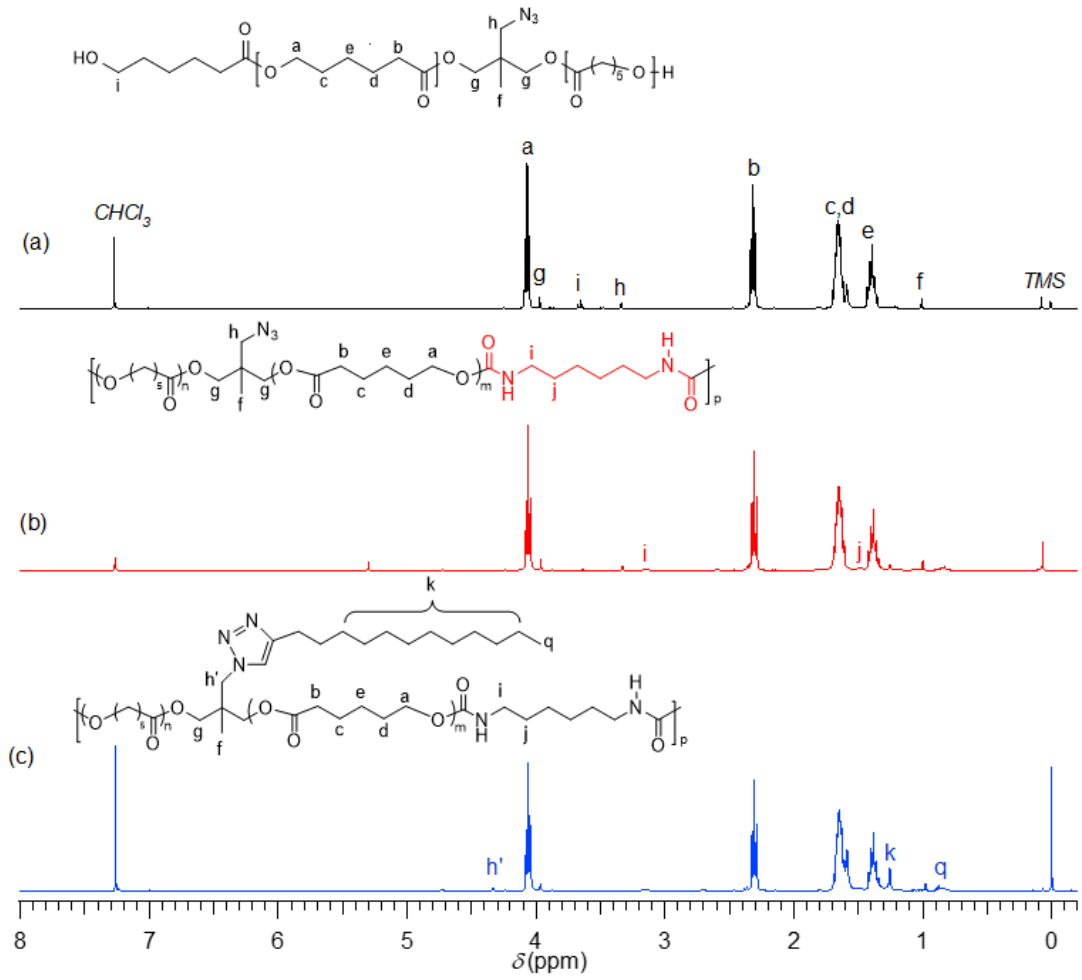

Figure S24. ^{1}H NMR spectra of PCL_{50}-N_3 (a), PU_{50}-N_3 (b) and PU_{50}-4 (c) determined in $CDCl_3$ at r.t.

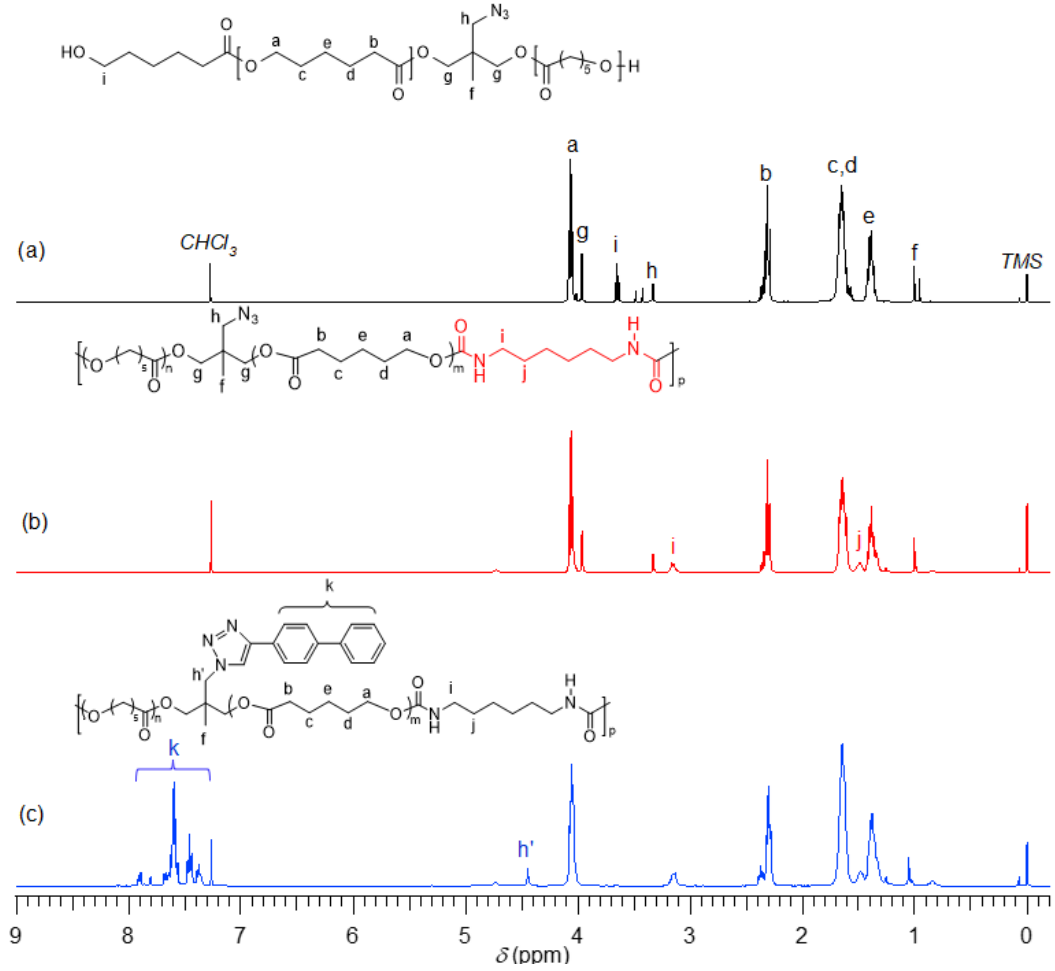

Figure S25. ^{1}H NMR spectra of PCL_{10}-N_3 (a), PU_{10}-N_3 (b) and PU_{10}-5 (c) determined in $CDCl_3$ at r.t.

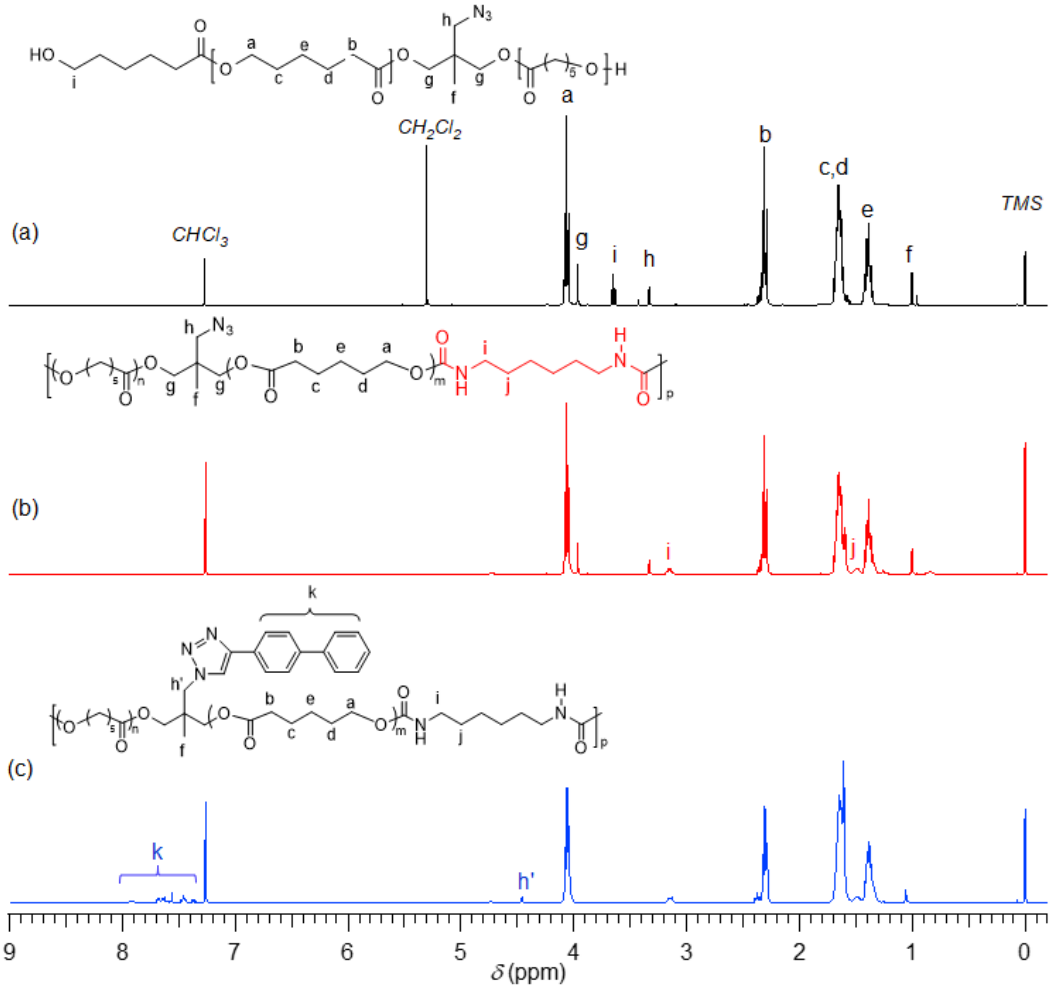

Figure S26. ^{1}H NMR spectra of PCL_{20}-N_3 (a), PU_{20}-N_3 (b) and PU_{20}-5 (c) determined in $CDCl_3$ at r.t.

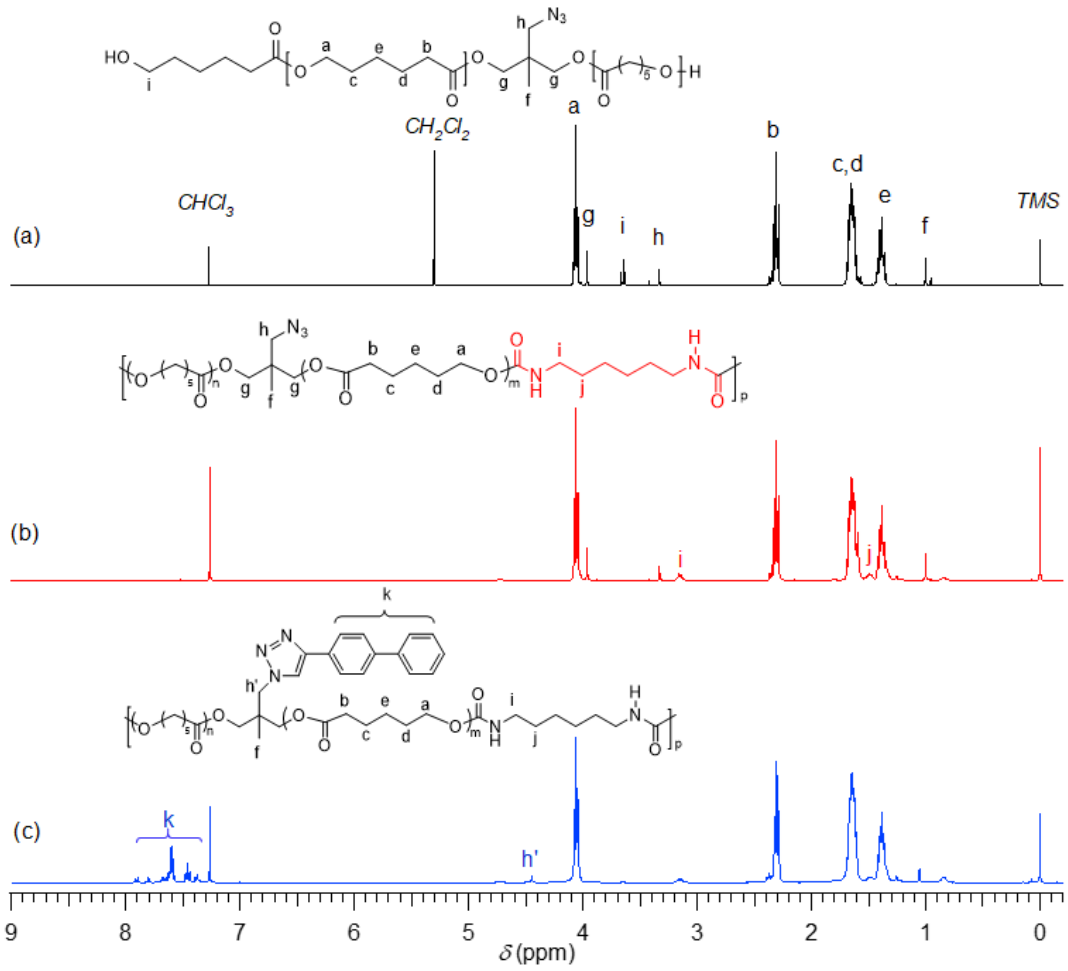

Figure S27. ^{1}H NMR spectra of PCL_{30}-N_3 (a), PU_{30}-N_3 (b) and PU_{30}-5 (c) determined in $CDCl_3$ at r.t.

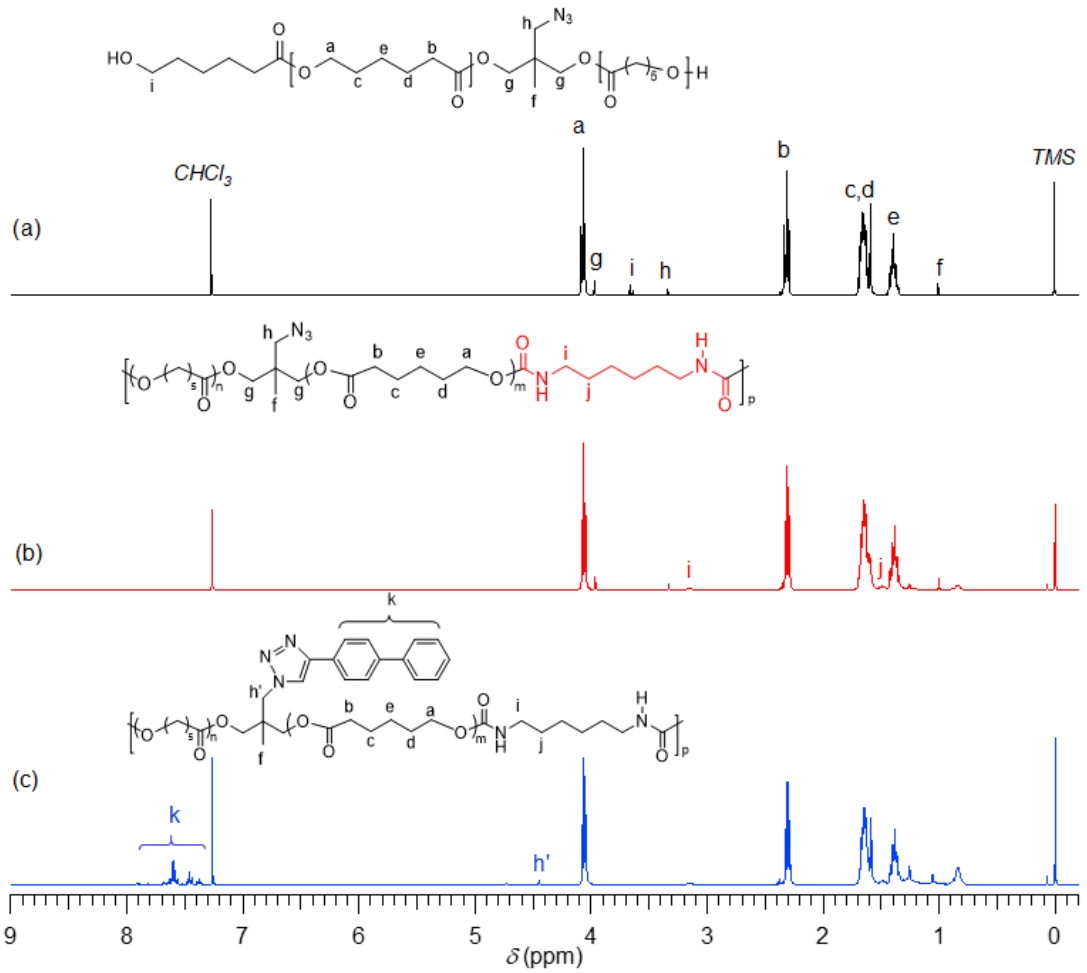

Figure S28. ^{1}H NMR spectra of PCL_{40}-N_3 (a), PU_{40}-N_3 (b) and PU_{40}-5 (c) determined in $CDCl_3$ at r.t.

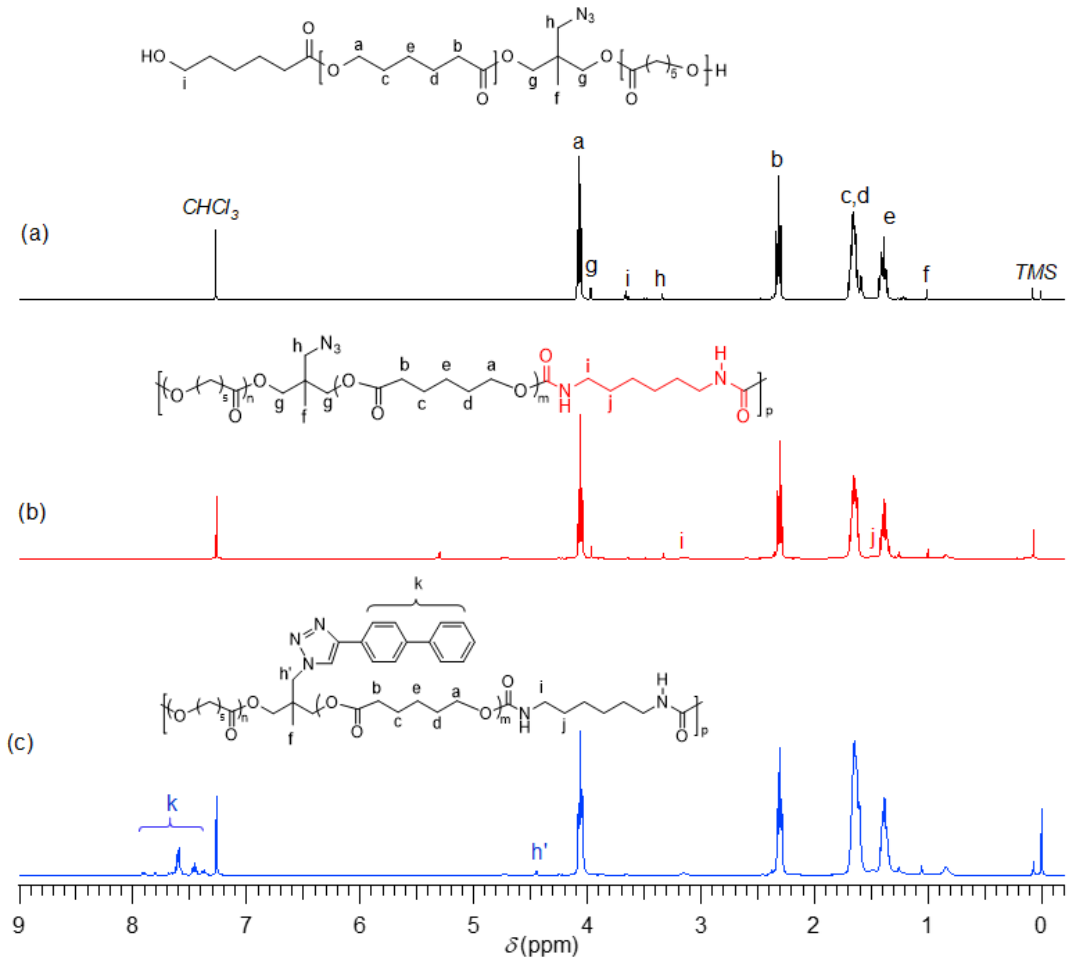

Figure S29. ^{1}H NMR spectra of PCL_{50}-N_3 (a), PU_{50}-N_3 (b) and PU_{50}-5 (c) determined in $CDCl_3$ at r.t.

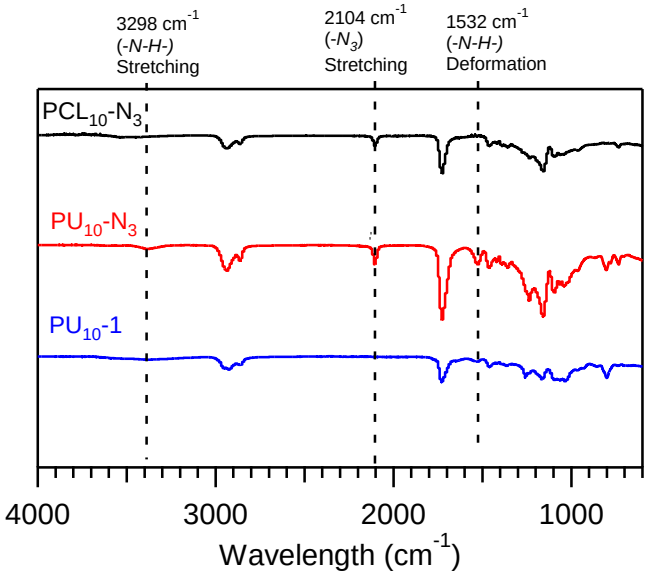

Figure S30. FT-IR spectra of PCL_{10}-N_3 (a), PU_{10}-N_3 (b) and PU_{10}-1 (c).

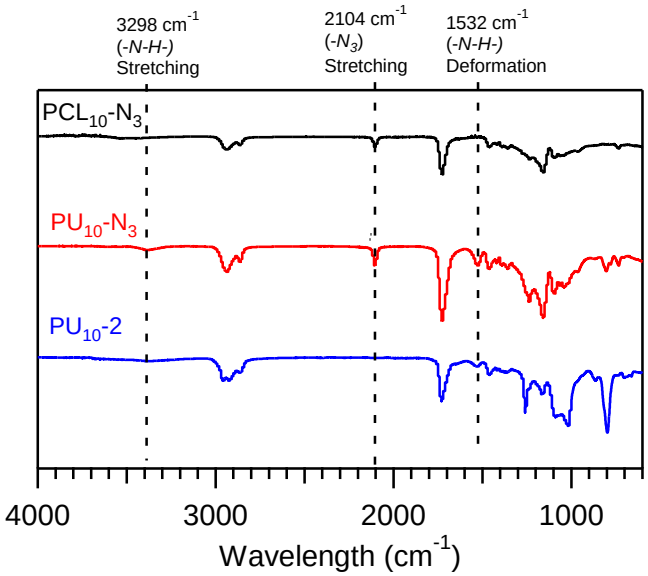

Figure S31. FT-IR spectra of PCL_{10}-N_3 (a), PU_{10}-N_3 (b) and PU_{10}-2 (c).

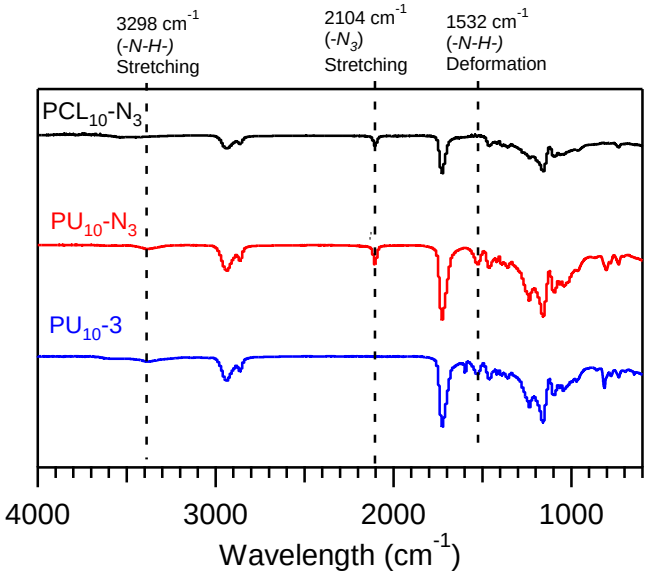

Figure S32. FT-IR spectra of PCL_{10}-N_3 (a), PU_{10}-N_3 (b) and PU_{10}-3 (c).

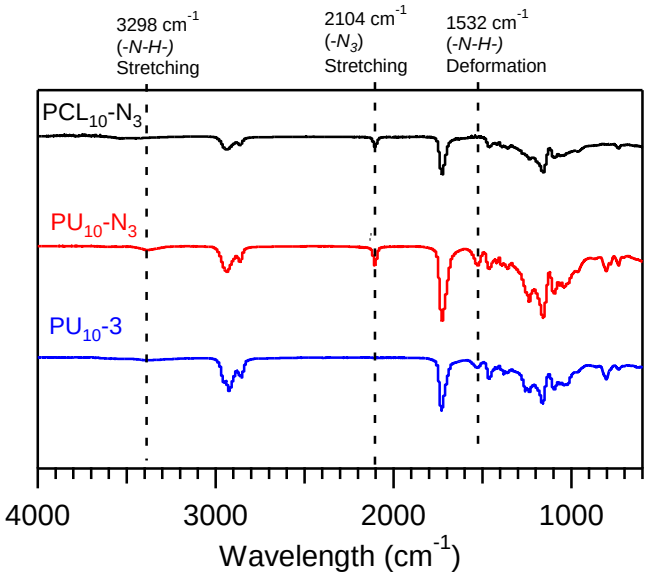

Figure S33. FT-IR spectra of PCL_{10}-N_3 (a), PU_{10}-N_3 (b) and PU_{10}-4 (c).

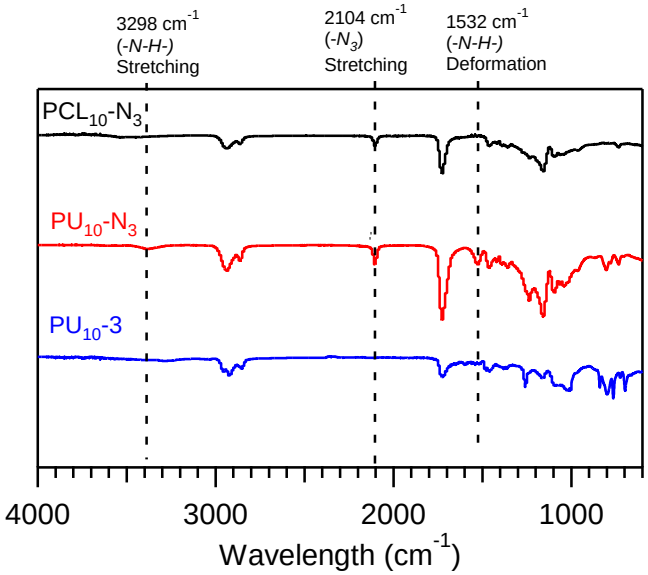

Figure S34. FT-IR spectra of PCL_{10}-N_3 (a), PU_{10}-N_3 (b) and PU_{10}-5 (c).

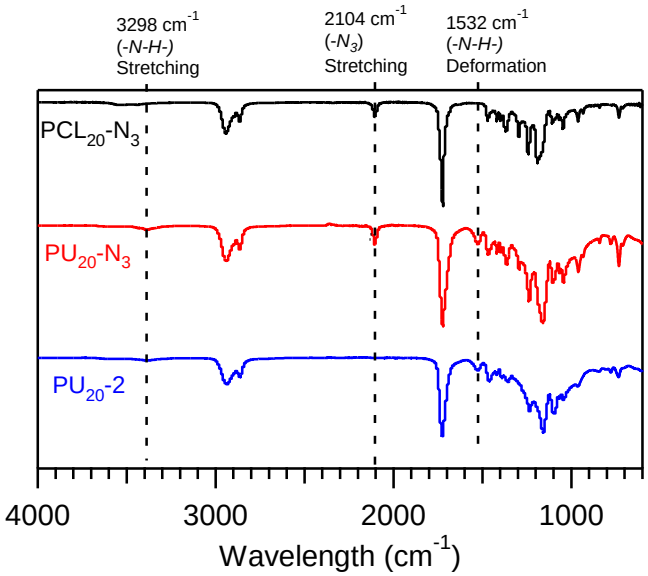

Figure S35. FT-IR spectra of PCL_{20}-N_3 (a), PU_{20}-N_3 (b) and PU_{20}-2 (c).

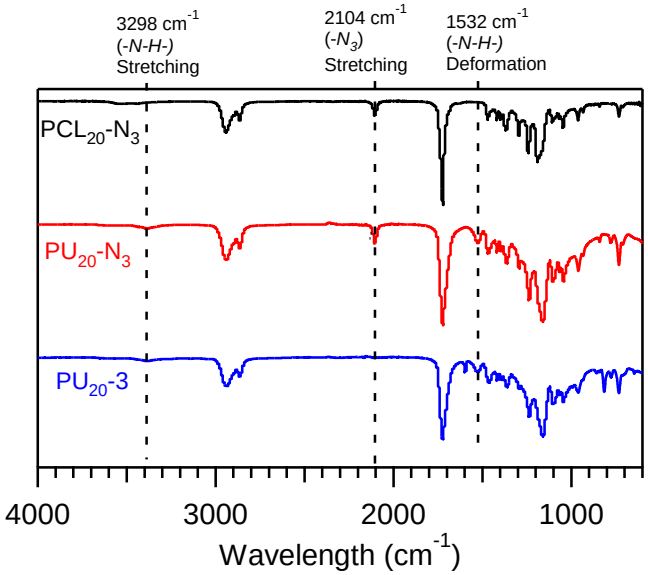

Figure S36. FT-IR spectra of PCL_{20}-N_3 (a), PU_{20}-N_3 (b) and PU_{20}-3 (c).

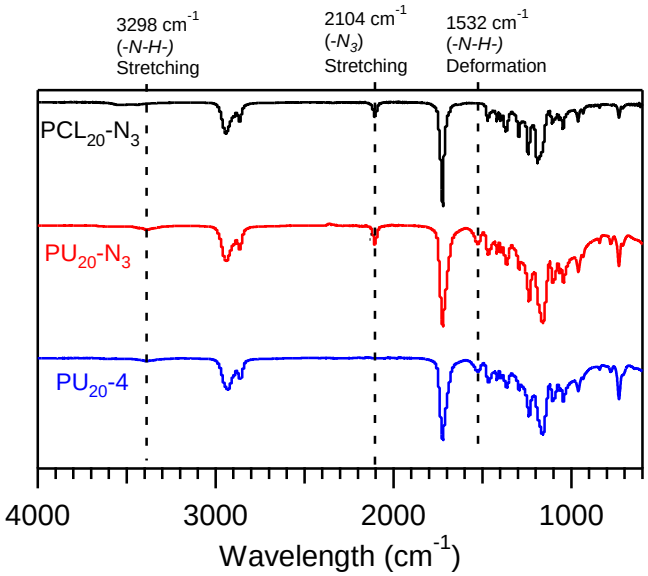

Figure S37. FT-IR spectra of PCL_{20}-N_3 (a), PU_{20}-N_3 (b) and PU_{20}-4 (c).

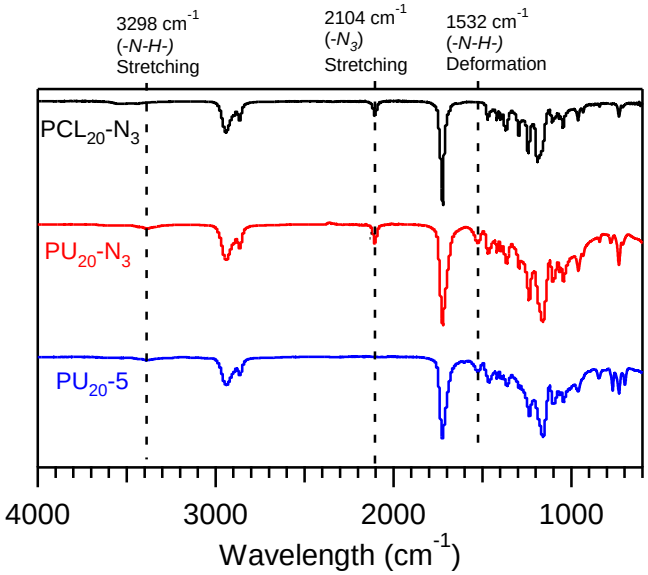

Figure S38. FT-IR spectra of PCL_{20}-N_3 (a), PU_{20}-N_3 (b) and PU_{20}-5 (c).

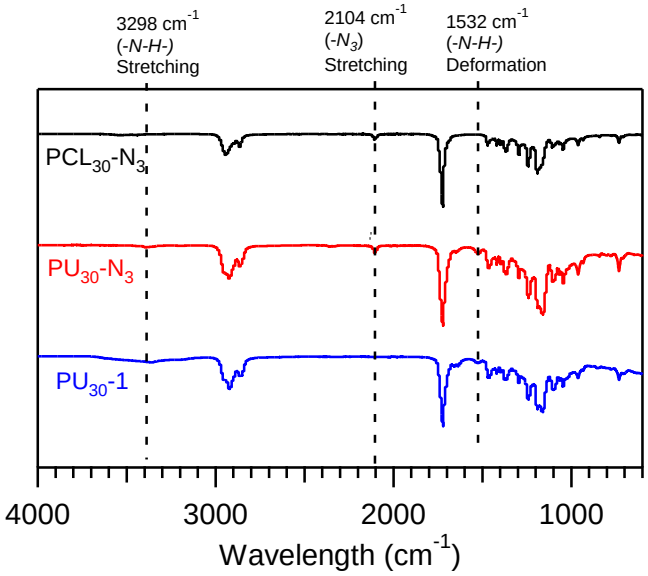

Figure S39. FT-IR spectra of PCL_{30}-N_3 (a), PU_{30}-N_3 (b) and PU_{30}-1 (c).

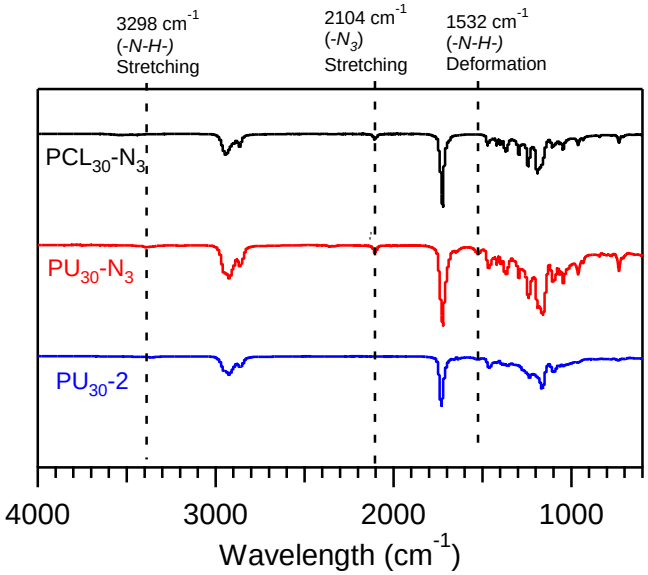

Figure S40. FT-IR spectra of PCL_{30}-N_3 (a), PU_{30}-N_3 (b) and PU_{30}-2 (c).

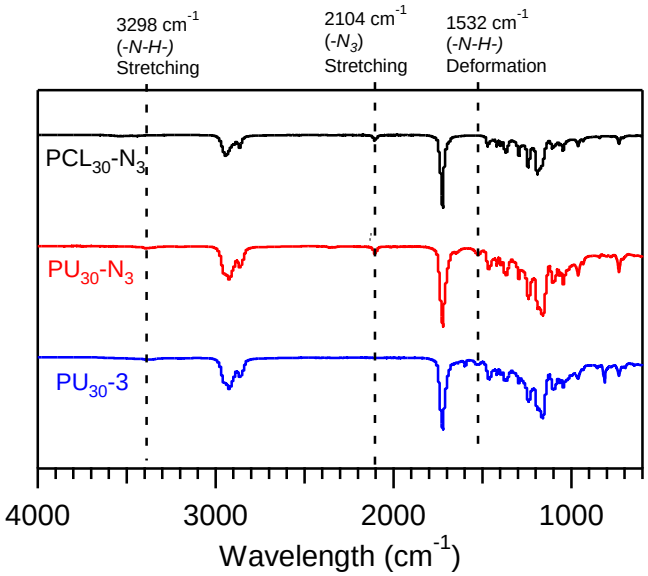

Figure S41. FT-IR spectra of PCL_{30}-N_3 (a), PU_{30}-N_3 (b) and PU_{30}-3 (c).

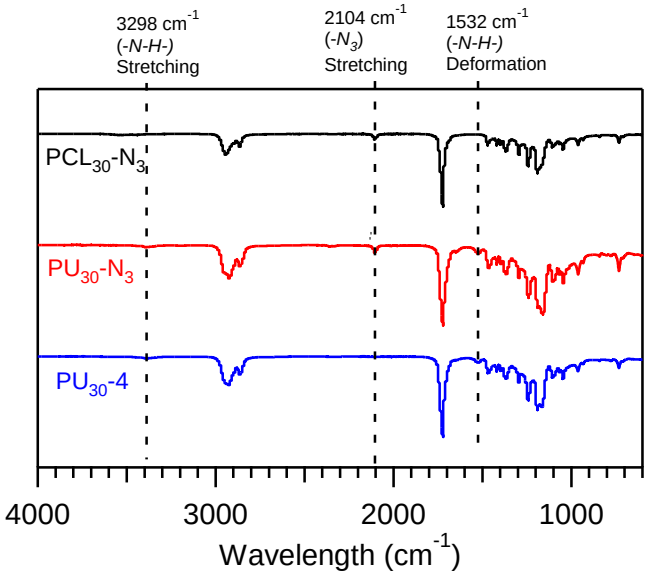

Figure S42. FT-IR spectra of PCL_{30}-N_3 (a), PU_{30}-N_3 (b) and PU_{30}-4 (c).

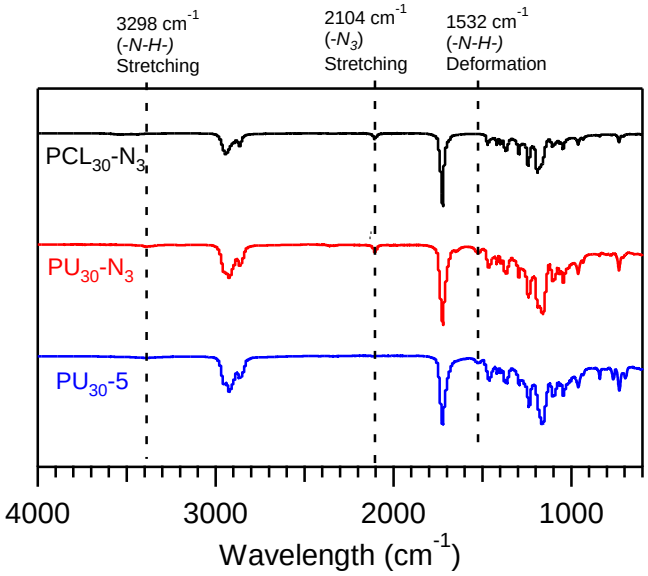

Figure S43. FT-IR spectra of PCL_{30}-N_3 (a), PU_{30}-N_3 (b) and PU_{30}-5 (c).

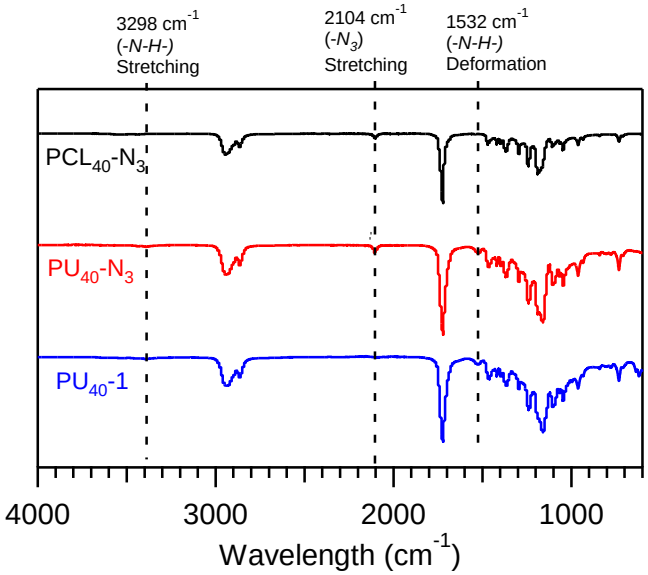

Figure S44. FT-IR spectra of PCL_{40}-N_3 (a), PU_{40}-N_3 (b) and PU_{40}-1 (c).

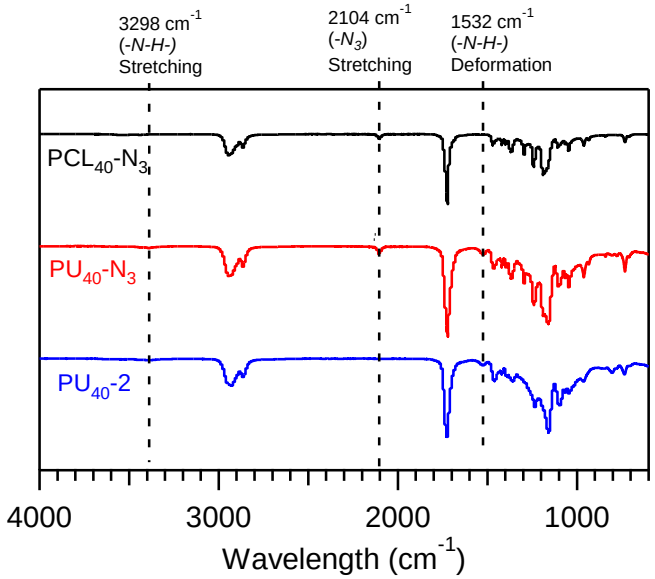

Figure S45. FT-IR spectra of PCL_{40}-N_3 (a), PU_{40}-N_3 (b) and PU_{40}-2 (c).

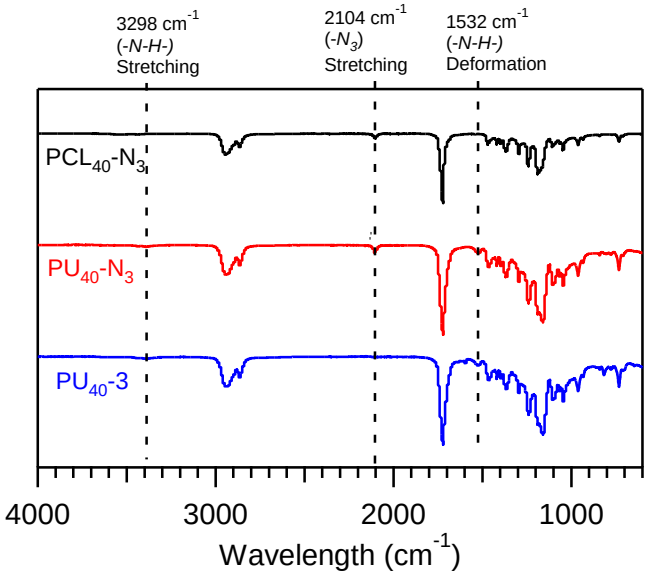

Figure S46. FT-IR spectra of PCL_{40}-N_3 (a), PU_{40}-N_3 (b) and PU_{40}-3 (c).

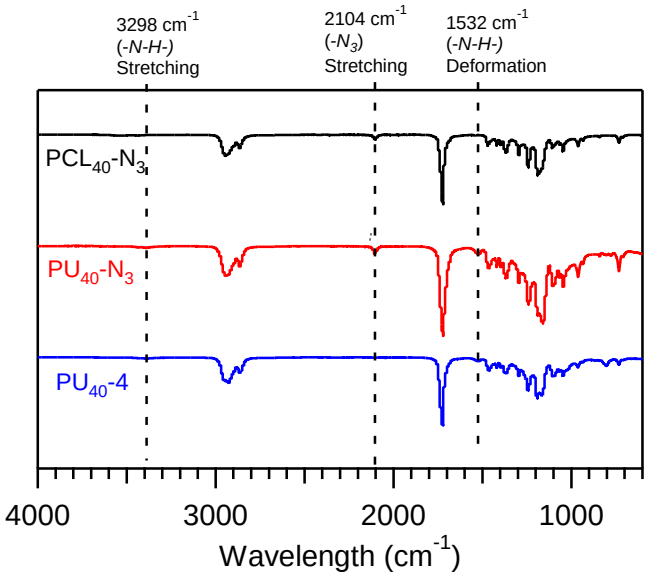

Figure S47. FT-IR spectra of PCL_{40}-N_3 (a), PU_{40}-N_3 (b) and PU_{40}-4 (c).

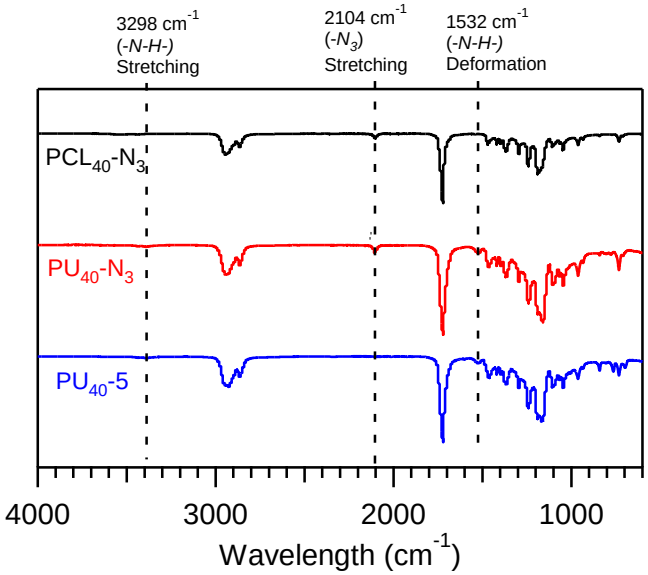

Figure S48. FT-IR spectra of PCL_{40}-N_3 (a), PU_{40}-N_3 (b) and PU_{40}-5 (c).

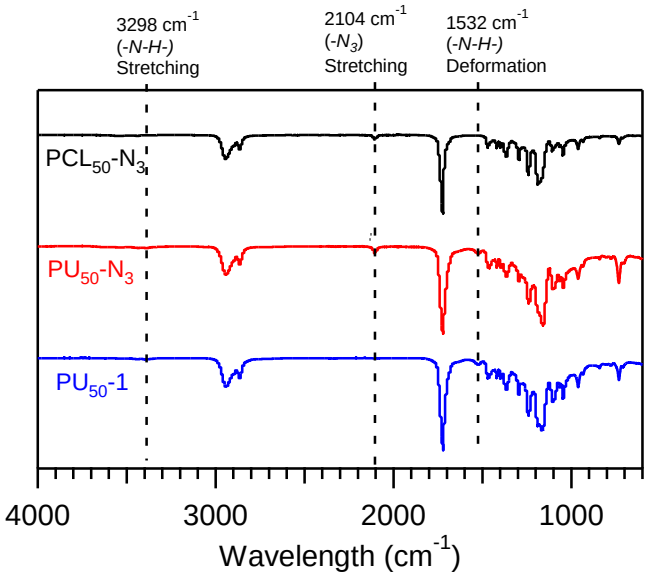

Figure S49. FT-IR spectra of PCL_{50}-N_3 (a), PU_{50}-N_3 (b) and PU_{50}-1 (c).

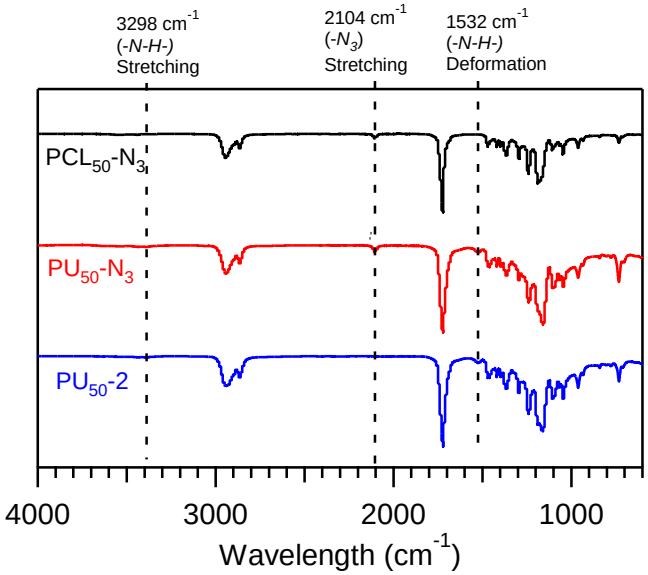

Figure S50. FT-IR spectra of PCL_{50}-N_3 (a), PU_{50}-N_3 (b) and PU_{50}-2 (c).

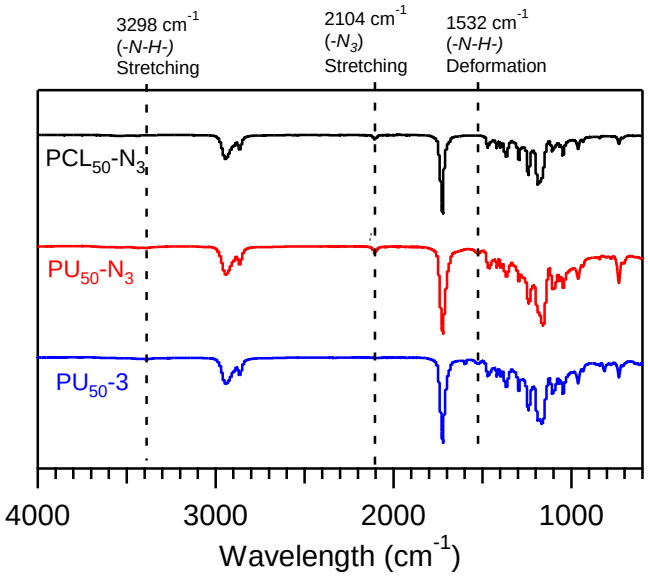

Figure S51. FT-IR spectra of PCL_{50}-N_3 (a), PU_{50}-N_3 (b) and PU_{50}-3 (c).

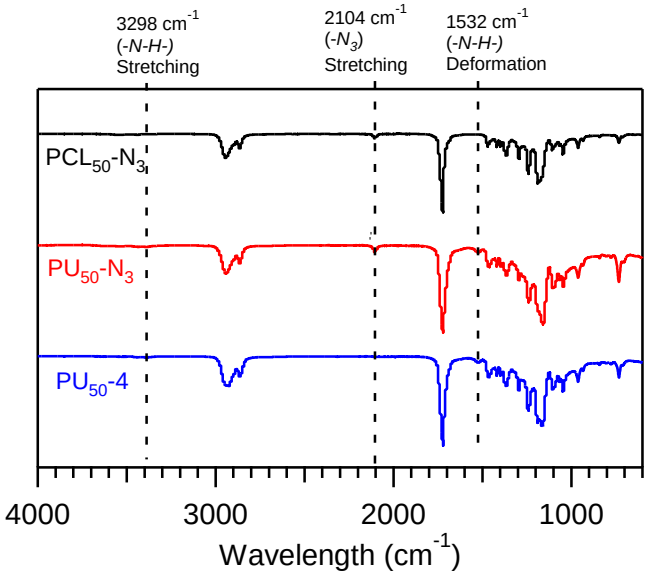

Figure S52. FT-IR spectra of PCL_{50}-N_3 (a), PU_{50}-N_3 (b) and PU_{50}-4 (c).

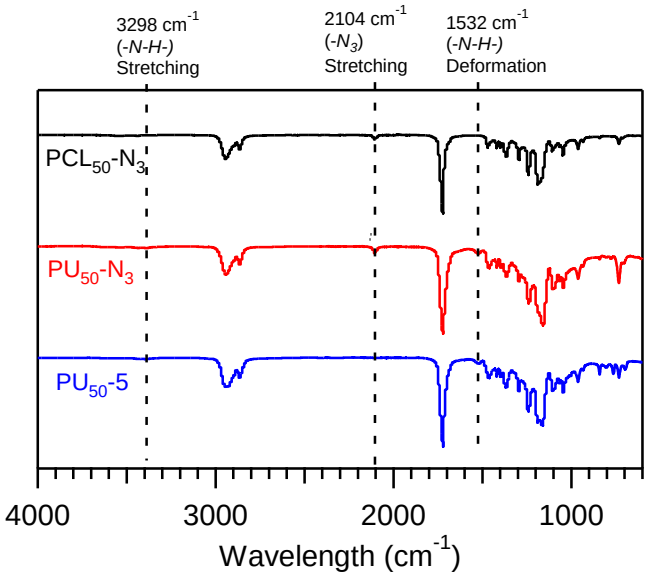

Figure S53. FT-IR spectra of PCL_{50}-N_3 (a), PU_{50}-N_3 (b) and PU_{50}-5 (c).

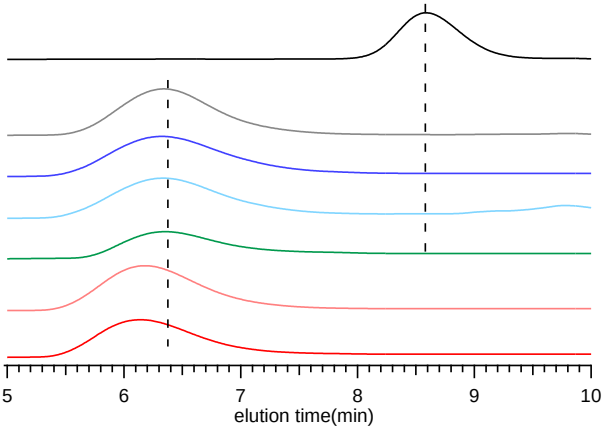

Figure S54. SEC traces of PCL_{10}-N_3 (black), PU_{10}-N_3 (grey), PU_{10}-**1** (blue), PU_{10}-**2** (light blue), PU_{10}-**3** (green), PU_{10}-**4** (light red), PU_{10}-**5** (red).

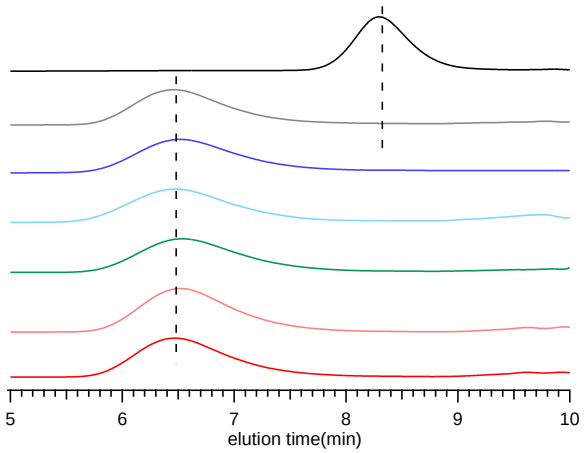

Figure S55. SEC traces of PCL_{20}-N_3 (black), PU_{20}-N_3 (grey), PU_{20}-**1** (blue), PU_{20}-**2** (light blue), PU_{20}-**3** (green), PU_{20}-**4** (light red), PU_{20}-**5** (red).

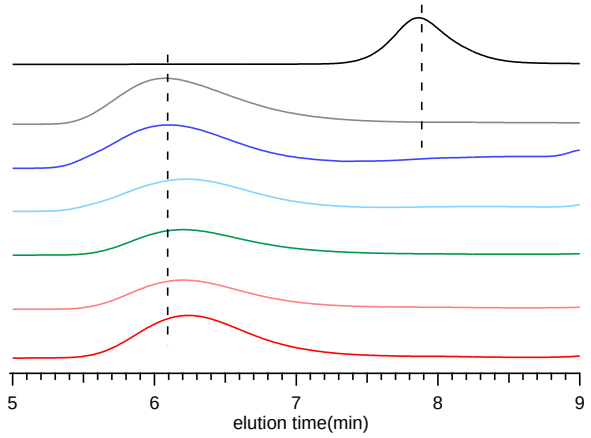

Figure S56. SEC traces of PCL_{40}-N_3 (black), PU_{40}-N_3 (grey), PU_{40}-**1** (blue), PU_{40}-**2** (light blue), PU_{40}-**3** (green), PU_{40}-**4** (light red), PU_{40}-**5** (red).

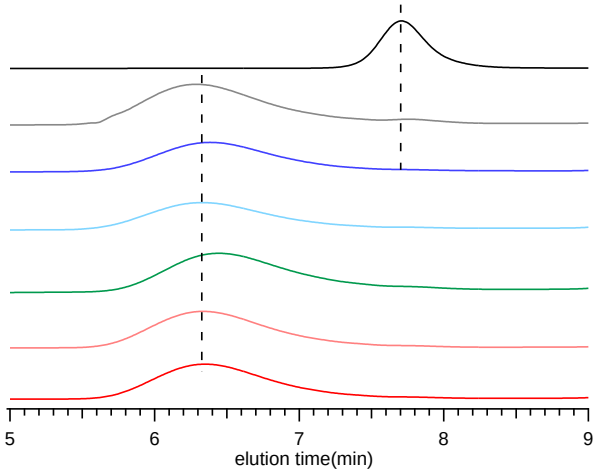

Figure S57. SEC traces of PCL_{50}-N_3 (black), PU_{50}-N_3 (grey), PU_{50}-**1** (blue), PU_{50}-**2** (light blue), PU_{50}-**3** (green), PU_{50}-**4** (light red), PU_{50}-**5** (red).

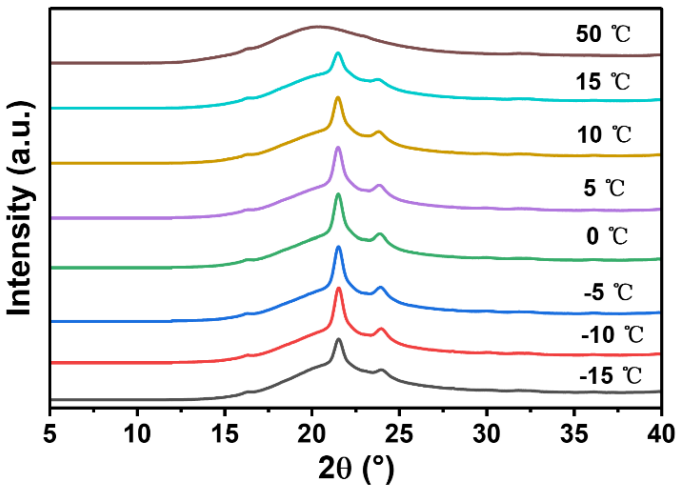

Figure S58. variable-temperature 1D WAXD profiles of PU_{10}-2 during the heating process from −15 to 50 °C at 5 °C min^{-1}.

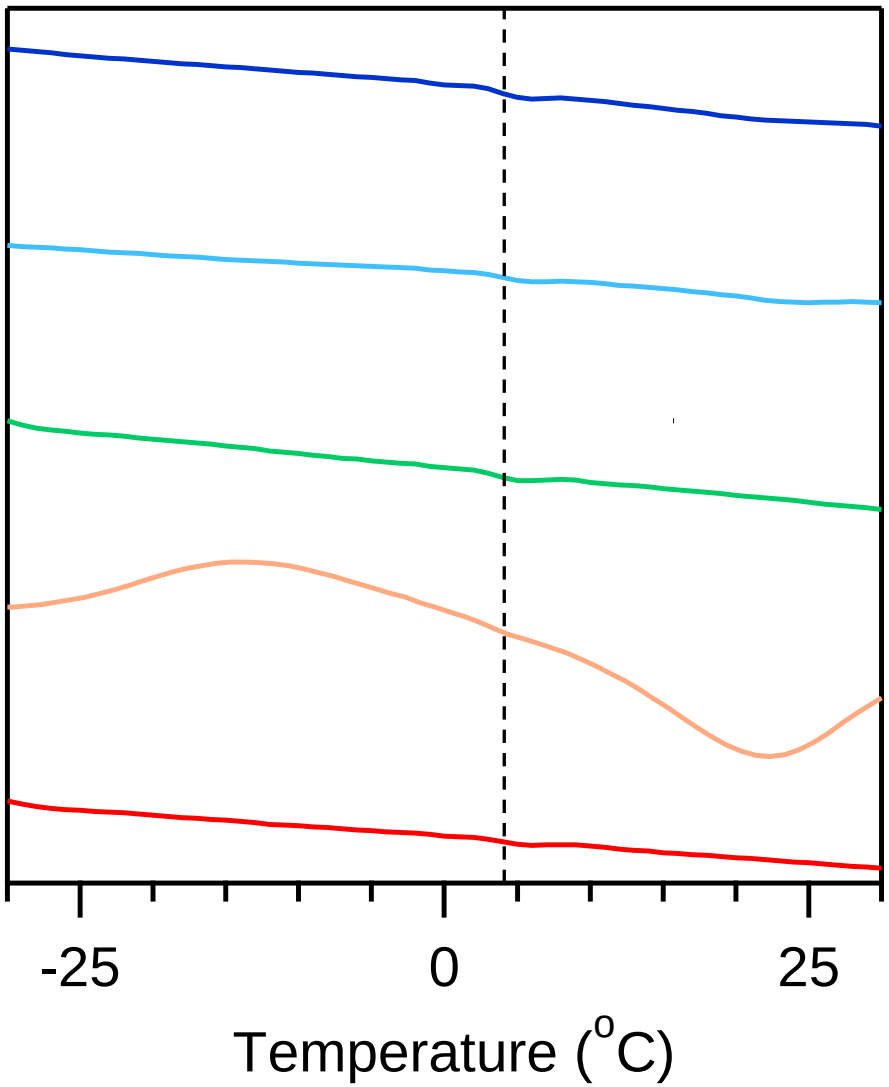

Figure S59. Expanded DSC profiles of PU_{10}s.

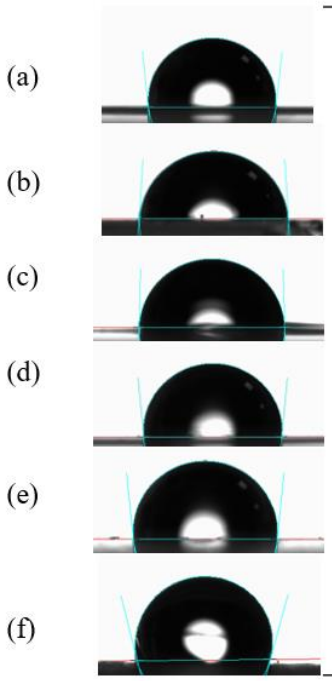

	Polyurethane	Contact angle (°)
(a)	PU_{10}	96.20
(b)	PU_{10}-1	85.1
(c)	PU_{10}-2	88.3
(d)	PU_{10}-3	95.5
(e)	PU_{10}-4	95.5
(f)	PU_{10}-5	104.7

Figure S60. Measurements of contact angle of deionized water on (a) PU_{10}-N_3, (b) PU_{10}-1, (c) PU_{10}-2, (d) PU_{10}-3, (e) PU_{10}-4, (f) PU_{10}-5.

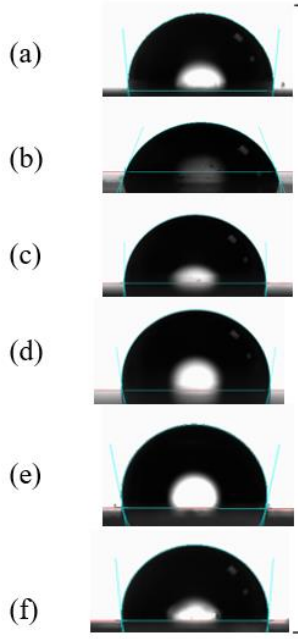

	PU	Contact angle (°)
(a)	PU_{20}	95.4
(b)	PU_{20}-1	68.4
(c)	PU_{20}-2	89.6
(d)	PU_{20}-3	98.2
(e)	PU_{20}-4	101.8
(f)	PU_{20}-5	95.8

Figure S61. Measurements of contact angle of deionized water on (a) PU_{20}-N_3, (b) PU_{20}-1, (c) PU_{20}-2, (d) PU_{20}-3, (e) PU_{20}-4, (f) PU_{20}-5.

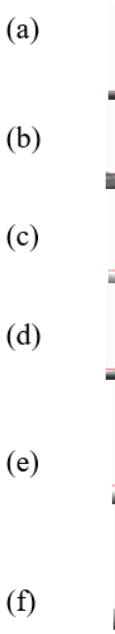

PU	Contact angle (°)
PU_{30}	90.10
PU_{30}-1	79.8
PU_{30}-2	83.0
PU_{30}-3	94.8
PU_{30}-4	117.0
PU_{30}-5	115.4

Figure S62. Measurements of contact angle of deionized water on (a) PU_{30}-N_3, (b) PU_{30}-1, (c) PU_{30}-2, (d) PU_{30}-3, (e) PU_{30}-4, (f) PU_{30}-5.

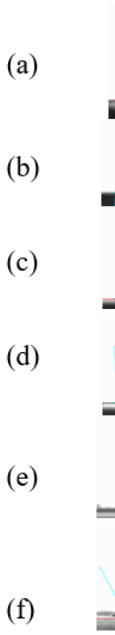

PU	Contact angle (°)
PU_{40}	90.2
PU_{40}-1	83.4
PU_{40}-2	87.2
PU_{40}-3	94.3
PU_{40}-4	101.6
PU_{40}-5	120.5

Figure S63. Measurements of contact angle of deionized water on (a) PU_{30}-N_3, (b) PU_{40}-1, (c) PU_{40}-2, (d) PU_{40}-3, (e) PU_{40}-4, (f) PU_{40}-5.

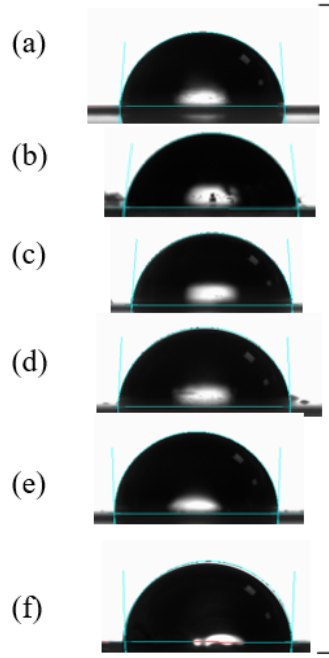

	PU	Contact angle (°)
(a)	PU_{50}	86.2
(b)	PU_{50}-1	83.2
(c)	PU_{50}-2	86.0
(d)	PU_{50}-3	87.5
(e)	PU_{50}-4	92.3
(f)	PU_{50}-5	91.8

Figure S64. Measurements of contact angle of deionized water on (a) PU_{30}-N_3, (b) PU_{50}-1, (c) PU_{50}-2, (d) PU_{50}-3, (e) PU_{50}-4, (f) PU_{50}-5.

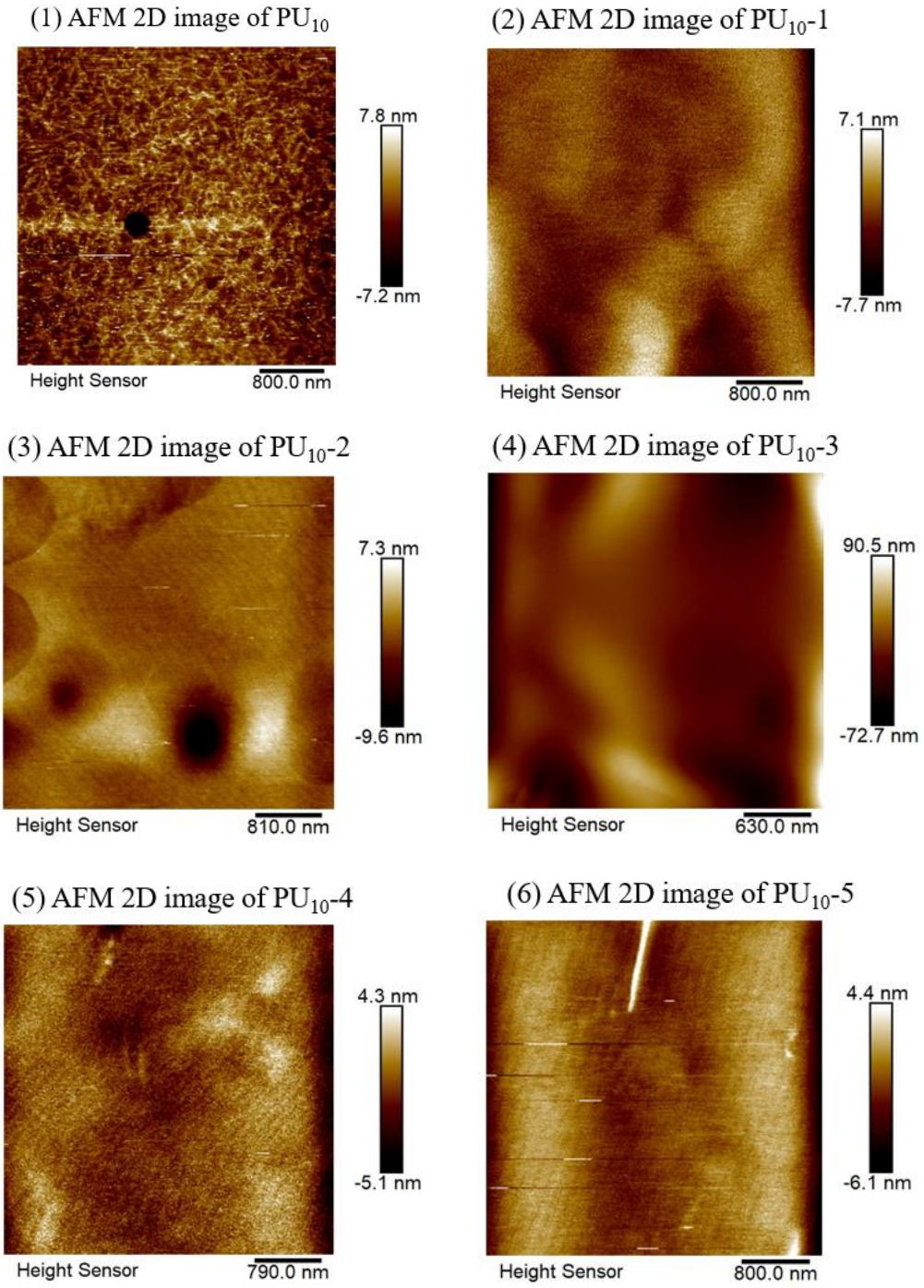

Figure S65. AFM spectra of PU_{10}-N_3, PU_{10}-1, PU_{10}-2, PU_{10}-3, PU_{10}-4, PU_{10}-5.

Table S1. The three-point tensile data of the synthetic polyurethane.

Entry	Test number	Young's Modulus (MPa) [a]	Tensile Stress (MPa) [b]	Elongation at Break (%) [c]	Toughness (MJ/m^3) [d]	Average stress (MPa)	Average strain (%)	Standard deviation of stress [e]	Standard deviation of strain [f]
PU_{10}-4	1	1.75	1.36	1330	8.64	0.88	1380	0.37	26
	2	1.86	0.622	1380	5.84				
	3	1.87	0.65	1440	5.72				
PU_{10}-5	1	6.05	1.54	1220	11.50	1.17	1190	0.27	95
	2	4.92	0.88	1290	7.97				
	3	2.86	1.10	1060	8.19				
PU_{30}-N_3	1	102	16.2	765	63.6	16.8	772	0.75	44
	2	124	15.9	721	69.7				
	3	117	17.6	830	82.9				
PU_{30}-1	1	137	22.9	1150	134	24.0	1090	0.96	49
	2	125	23.9	1090	138				
	3	143	25.2	1030	141				
PU_{30}-2	1	83.9	14.8	943	85.7	14.9	904	1.13	34
	2	84.4	17.1	874	84.4				
	3	73.9	12.6	895	67.9				
PU_{30}-3	1	164	18.3	890	90.8	18.2	837	2.51	38
	2	171	21.2	801	106.5				
	3	167	15.0	820	80.8				
PU_{30}-4	1	87.5	18.6	816	84.7	18.1	744	0.30	25
	2	72.8	18	777	80.9				
	3	126	17.9	755	90.1				
PU_{30}-5	1	187	16.3	754	83.9	15.0	744	0.90	56
	2	180	14.6	670	71.3				
	3	193	14.2	808	79.2				
PU_{50}-N_3	1	129	18.8	750	91.9	18.6	747	0.46	17
	2	180	19.0	767	104				
	3	218	17.9	725	83.0				
PU_{50}-1	1	102	21.0	990	126	25.3	912	3.43	23
	2	143	29.4	990	177				
	3	175	25.6	940	151				
PU_{50}-2	1	140	25.6	1020	124	24.0	912	2.11	96
	2	141	25.5	923	12				
	3	121	21.0	789	88.6				
PU_{50}-3	1	160	13.2	841	68.8	14.2	785	0.76	40
	2	180	14.9	750	71.7				
	3	177	14.5	763	69.5				
PU_{50}-4	1	177	17.8	906	88.0	16.8	943	0.80	28
	2	153	15.8	976	76.4				
	3	141	16.9	948	87.8				
PU_{50}-5	1	148	19.3	813	86.9	18.5	814	0.66	1
	2	158	18.6	816	92.9				
	3	148	17.7	813	81.6				

[a] Calculated from the initial linear region of stress–strain curves.
[b] Determined as the maximum stress during tensile testing.
[c] Determined as the percentage strain at sample fracture.
[d] Calculated from the integral area under stress–strain curves.
[e] Standard deviation of tensile stress from three parallel measurements.
[f] Standard deviation of strain at break from three parallel measurements.

References

1. P. Chandra, A. M. Jonas, A. E. Fernandes, Sequence and Surface Confinement Direct Cooperativity in Catalytic Precision Oligomers. *J. Am. Chem. Soc.*, **2018**, *140* (15), 5179-5183.
2. J. Niskanen, M. N. Tousignant, A. J. Peltekoff, B. H. Lessard, Poly(ethylene glycol)-Based Poly(ionic liquid) Block Copolymers through 1,2,3-Triazole Click Reactions. *ACS Appl. Polym. Mater.*, **2022**, *4* (03), 1559-1564.
3. P. C. Chen, V. Patil, W. Guerrant, P. Green, A. K. Oyelere, Synthesis and structure–activity relationship of histone deacetylase (HDAC) inhibitors with triazole-linked cap group. *Bioorg. Med. Chem*., **2008**, *16* (09), 4839-4853.